

# Geochemistry, Geophysics, Geosystems

## RESEARCH ARTICLE

10.1029/2018GC007923

### Key Points:

- This study documents hydrous subduction related magmatism throughout the Oman-UAE ophiolite
- Amphibole fractionation played an important role during the formation of this type of magmatism
- These observations strongly suggest the Oman-UAE ophiolite formed in a suprasubduction zone setting

### Supporting Information:

- Supporting Information S1
- Data Set S1
- Data Set S2
- Data Set S3

### Correspondence to:

S. J. de Graaff,  
sietze.de.graaff@vub.be

### Citation:

de Graaff, S. J., Goodenough, K. M., Klaver, M., Lissenberg, C. J., Jansen, M. N., Millar, I., & Davies, G. R. (2019). Evidence for a moist to wet source transition throughout the Oman-UAE ophiolite, and implications for the geodynamic history. *Geochemistry, Geophysics, Geosystems*, 20, 651–672. <https://doi.org/10.1029/2018GC007923>

Received 24 AUG 2018








Accepted 28 DEC 2018

Accepted article online 5 JAN 2019

Published online 1 FEB 2019

©2019. American Geophysical Union.  
All Rights Reserved.

## Evidence for a Moist to Wet Source Transition Throughout the Oman-UAE Ophiolite, and Implications for the Geodynamic History

S. J. de Graaff<sup>1,2</sup> , K. M. Goodenough<sup>3</sup> , M. Klaver<sup>4</sup> , C. J. Lissenberg<sup>5</sup> , M. N. Jansen<sup>1,5</sup> , I. Millar<sup>6</sup> , and G. R. Davies<sup>1</sup> 

<sup>1</sup>Faculty of Science, Vrije Universiteit Amsterdam, Amsterdam, Netherlands, <sup>2</sup>Analytical, Environmental and Geochemistry, Vrije Universiteit Brussel, Elsene, Belgium, <sup>3</sup>British Geological Survey, the Lyell Centre, Edinburgh, UK, <sup>4</sup>School of Earth Sciences, University of Bristol, Wills Memorial Building, Bristol, UK, <sup>5</sup>School of Earth and Ocean Sciences, Cardiff University, Cardiff, UK, <sup>6</sup>British Geological Survey, Nottingham, UK

**Abstract** The Oman-United Arab Emirates (UAE) ophiolite represents the largest and best-preserved fragment of obducted oceanic lithosphere in the world. However, debate continues regarding its geodynamic history. This debate is in part a consequence of the lateral variability in the later stage magmatic units, with arc signatures considered to be well developed in the north of the ophiolite but less so in the south. In this study, we investigate later stage intrusions in the central and southern part of the ophiolite. These intrusions vary from wehrlite to gabbro and tonalite and crosscut all levels of the main ophiolite sequence from the mantle peridotites up to the sheeted dike complex. They are characterized by the presence of magmatic amphibole, low TiO<sub>2</sub> (<1 wt%), document an enrichment in Th, Sr, and Ba, depletion of Y and Dy, and decreasing Dy/Yb and Dy/Dy\* with increased fractionation. These data record hydrous fractionation with a significant role for amphibole, which is comparable to many arc-type magmas. The relative Nb and light rare earth element ((La/Yb)<sub>n<sub>chon</sub></sub> < 1) depletion and coupled Nd and Hf isotope variations indicate the same (but depleted) Indian mid-ocean ridge basalts-type mantle source as the main ophiolite sequence. More radiogenic Pb isotope compositions of plagioclase imply the addition of a fluid component likely derived from sediments or altered oceanic crust. These intrusions occur across larger areas than previously reported, implying the entire ophiolite formed in a setting characterized by arc-type magmas, such as a suprasubduction zone setting.

### 1. Introduction

The Oman-United Arab Emirates (UAE; or Semail) ophiolite is regarded as one of the best-preserved pieces of oceanic crust in the world, comprising the remnants of Tethyan oceanic lithosphere that was obducted onto the Arabian Shield during the Late Cretaceous (e.g., Ernewein et al., 1988; Lippard et al., 1986; Rioux et al., 2012, 2013). The ophiolite shows remarkably little deformation and consists of 12 fault-bounded blocks (Figure 1) with a well-exposed Penrose Conference sequence (Anonymous, 1972) of mantle ultramafic rocks, layered and high-level gabbros, and a sheeted dike complex with associated pillow lavas (Lippard et al., 1986). The geodynamic setting in which the Oman-UAE ophiolite formed is debated. Initially considered a perfect example of crust formed at a mid-ocean ridge (Coleman, 1981), analogies were made to crust formed at a fast-spreading center (Nicolas et al., 1996). However, depleted arc tholeiites were recorded by some early workers, leading to the suggestion of a suprasubduction zone (SSZ) setting (Alabaster et al., 1982; Pearce et al., 1981). Subsequently, later stage magmatic sequences in the northern part of the ophiolite were recognized to have a boninitic affinity (Ishikawa et al., 2002) and originate from a hydrated source (Goodenough et al., 2010), suggesting that at least part of the ophiolite formed in a SSZ environment (see Goodenough et al., 2014 for an overview). Furthermore, recent work has suggested that the main gabbro-sheeted dike-pillow lava sequence of the ophiolite formed from “moist” magmas (0.1–1 wt% H<sub>2</sub>O), indicative of a SSZ origin for the entire ophiolite (MacLeod et al., 2013). These arguments notwithstanding, the geochemical composition of the ophiolite’s main crustal sequence is, with a few exceptions (e.g., Lachize et al., 1996; Wadi Haymilyah), similar to normal mid-ocean ridge basalts (N-MORB; comparable to that formed at the East Pacific Rise; Nicolas, 1989). The main ophiolite sequence only documents a weak trace element signature of subduction that some propose originated from remnants of

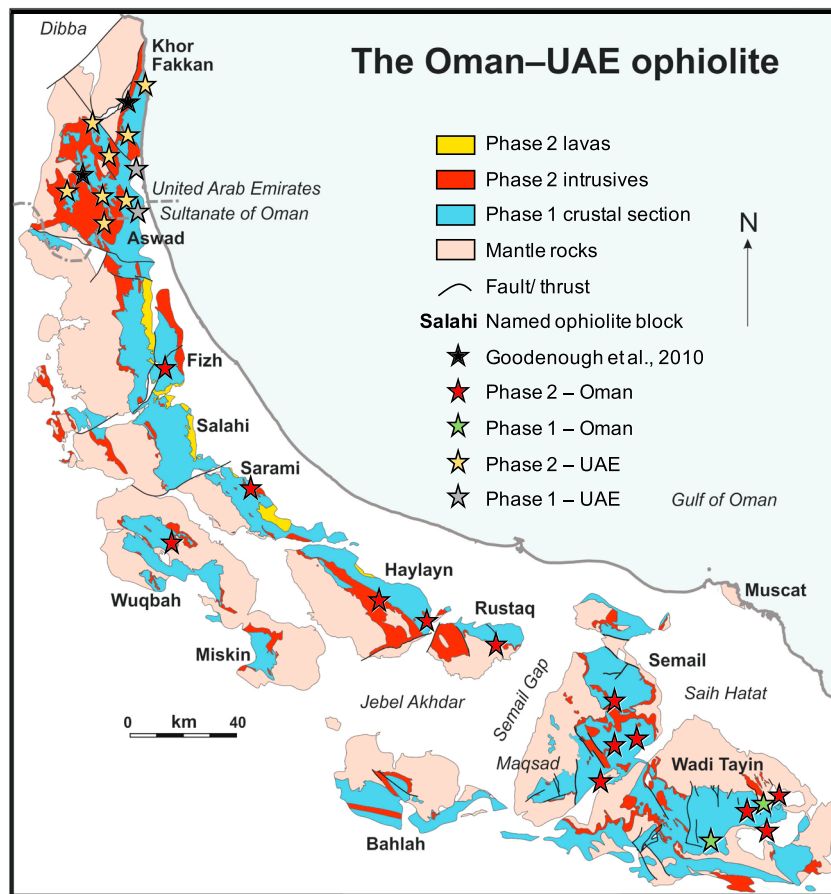


**Figure 1.** Map of Oman with sample locations denoted with stars (adapted from Goodenough et al., 2014, and used with permission). UAE = United Arab Emirates.

ancient subducted material in the source region, similar to a present-day Indian MORB source (e.g., Godard et al., 2006; Mahoney et al., 1998).

The dichotomy in geochemical characteristics between the main crustal sequence and later stage magmatic sequences has been explained as either evolution of the magmatic setting from a spreading ridge to a SSZ setting (e.g., Goodenough et al., 2014; Nicolas & Boudier, 2015, and references therein), a consequence of the initiation of obduction (Ernewein et al., 1988; Godard et al., 2006), or melting of the ophiolite's crust through seawater penetration (Abily et al., 2011; Benoit et al., 1999; Bosch et al., 2004; Boudier et al., 2000). Additionally, the significance of later stage magmatism was often downplayed (e.g., Nicolas & Boudier, 2011; Nicolle et al., 2016) until recently due to the lack of description of pervasive later stage intrusive (and extrusive) magmatism in the southern part of the ophiolite (the blocks east of the Semail Gap; Figure 1; Haase et al., 2016; Müller et al., 2017). This apparent lack of later stage intrusions, coupled with more MORB-type compositions of the main crustal sequence toward the south (Python et al., 2008), was generally regarded as evidence for a MOR origin of the southern part of the ophiolite. However, the recent report of plagiogranites in both the central and southern part of the ophiolite (Haase et al., 2016), similar to the late stage intrusions described by Goodenough et al. (2010), suggests that later stage magmatism may be more common in the southern part of the ophiolite than previously believed. In this paper, we document late crosscutting intrusions in the central and southern part of the ophiolite. Through petrographical and geochemical analyses we investigate their relation to other magmatic sequences within the ophiolite and provide evidence for the hypothesis that later stage, SSZ-type magmatism is more widespread in the Oman-UAE ophiolite than previously appreciated.

## 2. Geological and Magmatic History

The Oman-UAE ophiolite is part of the Hajar Mountain Range, which extends roughly 500 km along the northeastern coast of the Arabian Peninsula (Figure 1) and belongs to the Alpine-Himalayan fold belt (Lippard et al., 1986). The ophiolite comprises 12 fault-bounded blocks, of which 3 occur in the UAE to the north, and the rest in Oman (Figure 1). Dating of the metamorphic sole of the ophiolite suggests that obduction onto the Upper Proterozoic basement of the Arabian Shield initiated around 94 Ma (Hacker et al., 1996; Warren et al., 2005). Initial formation of the ophiolite predates this event by approximately 2 Myr, with the earliest and later stages of magmatism largely formed between 96.5 and 94 Ma (Goodenough et al., 2010; Rioux et al., 2012, 2013; Warren et al., 2005). Folding on large upright axial planes and local thrust reactivation during Post-Miocene uplift marks the last major tectonic event, which formed the current topographic elevation (Lippard et al., 1986).

Numerous workers have described the different phases and types of magmatism within the Oman-UAE ophiolite (e.g., Adachi & Miyashita, 2003; Alabaster et al., 1982; Boudier & Juteau, 2000; Ernewein et al., 1988; Goodenough et al., 2010, 2014; Haase et al., 2015, 2016; Koga et al., 2001; Pearce et al., 1981; Python & Ceuleneer, 2003; Rollinson, 2009, 2015; Styles et al., 2006; Yamasaki et al., 2006). Several different magmatic phases have been recognized and classified: the Geotimes, Lasail, Alley, clinopyroxene-phyric, and Salahi units (Alabaster et al., 1982; Pearce et al., 1981); V1, V2, and V3 (Ernewein et al., 1988); and Phases 1 and 2 (Goodenough et al., 2014; Haase et al., 2016). Due to the variable spatial distribution of the magmatic sequences, with later stage extrusive rocks being apparently less common in the southern part of the ophiolite (Godard et al., 2003; Nicolle et al., 2016), the relationship between the different intrusive and extrusive units described in the literature is not always clear. For example, many intrusions have been attributed to the earliest phase of magmatism (Adachi & Miyashita, 2003; Dilek & Flower, 2003; Juteau et al., 1988; Shervais, 2001; Yamasaki et al., 2006) even though associated extrusives may be attributed to later episodes, likely because crosscutting relationships are not visible at the outcrop scale. This study follows the terminology of Goodenough et al. (2014) who used field data, geochemical, and mineralogical differences to define Phase 1 and Phase 2 magmatism. We propose the term Phase 3 for the latest, Salahi-type magmatism.

Phase 1 comprises the upper mantle ultramafic rocks and the early crustal succession of layered gabbros, high-level gabbros, and the sheeted dike complex with associated pillow lavas (referred to as the Geotimes lavas of Alabaster et al., 1982, or the V1 of Ernewein et al., 1988). The mantle section of the ophiolite passes upward into the crustal succession via the Moho Transition Zone (MTZ) which, in Phase 1, is dominated by dunite and gabbro (Koga et al., 2001). The relatively low incompatible element abundance and positive Sr and Eu anomalies demonstrate the layered and high-level gabbros of the Phase 1 crustal section to be typical of cumulates such as those formed at spreading centers (Garrido et al., 2001; MacLeod & Yaouancq, 2000; Pallister & Knight, 1981). The sheeted dike complex and pillow lavas, which have not been affected by crystal accumulation, provide the best representation of magmatic compositions (MacLeod et al., 2013). The sheeted dikes and lavas have relative Nb and Ta depletion and show major and minor element trends typical for tholeiites with elevated water contents, all of which are consistent with a marginal basin setting (Goodenough et al., 2014; MacLeod et al., 2013). The relatively homogeneous stratigraphic succession and spreading rates determined in multiple studies (e.g., Nicolas & Boudier, 2015, and references therein) suggest that Phase 1 magmatism formed at a fast-spreading center regardless of geodynamic setting (Godard et al., 2006). Dating of the sequence suggests Phase 1 formed between 96.5 and 95.5 Ma (Rioux et al., 2012, 2013).

Phase 2 is clearly defined by a crosscutting magmatic sequence of wehrlites, gabbros, leucogabbros, plagiogranites (which include tonalites and trondhjemites; Rollinson, 2009), and basaltic to basaltic andesite dikes and lavas, which typically have a higher Mg# at similar SiO<sub>2</sub> wt% and a depleted incompatible element signature compared to Phase 1 (Godard et al., 2006). These Phase 2 magmas likely originated from a hydrated source from which some melt had already been extracted (Alabaster et al., 1982; Godard et al., 2003; Goodenough et al., 2014; Koga et al., 2001), which is apparent in more pronounced negative Nb and Ta anomalies, and light rare earth element (LREE) depletion compared to Phase 1. In addition, Phase 2 is marked by generally lower whole rock TiO<sub>2</sub> (<1 wt%), more calcic rather than sodic plagioclases, and clinopyroxene with lower TiO<sub>2</sub>, Na<sub>2</sub>O, and Al<sub>2</sub>O<sub>3</sub> at a given Mg# (Adachi & Miyashita, 2003; Goodenough et al.,

2010; Yamasaki et al., 2006). The Lasail, Alley, and clinopyroxene-phyric volcanic units (Alabaster et al., 1982), the V2 lavas (Ernewein et al., 1988), boninites (Ishikawa et al., 2002), and the later stage intrusions described by Goodenough et al. (2010) and Haase et al. (2016) are regarded as Phase 2 magmatism. They are considered to represent an off-axis, post-spreading stage of magmatism that intruded the ophiolite between 95.4 and 95.1 Ma (Goodenough et al., 2010; Rioux et al., 2012, 2013), postdating the Phase 1 sequence by less than 1 Myr. In the north of the ophiolite, Phase 2 magmatism can represent up to 50% of the exposed area of ophiolite crust, but it is generally considered to be much less abundant in the southern blocks (Goodenough et al., 2014).

A third, off-axis phase of magmatism has been described as the Salahi unit (Alabaster et al., 1982; Ernewein et al., 1988; Lippard et al., 1986) or the late enriched magmatism (Goodenough et al., 2010). This phase, which is relatively small in volume, includes crosscutting basaltic to microgabbro intrusions that typically show a general incompatible element enrichment and marked enrichment in the fluid mobile elements Rb, K, and Pb. These intrusions are associated with later granitoids that contain a component of sediment-derived melt (Haase et al., 2015; Rollinson, 2015; Styles et al., 2006). Whether the latter represent melting of continental margin sediments by the hot overriding ophiolite or subduction-derived melts is debated (Ernewein et al., 1988; Haase et al., 2015; Rollinson, 2015) and, with the focus of this study being on Phase 2 magmatism, is a subject beyond the scope of this paper. Nevertheless, Phase 3 magmatism records a significantly different history to the majority of Phase 2 magmatism, and with ages varying between 95.5 and 94 Ma (Rioux et al., 2013; Warren et al., 2005), they undoubtedly represent the youngest intrusions documented in the ophiolite.

### 3. Phase 2 Magmatism: Field Relations

The Phase 2 intrusions described here have many forms, from distinct dikes with chilled margins (up to 3 m wide), to sill-like structures and larger intrusive sheets >10 m across (Figure 2). Phase 2 intrusions occur at all levels within the ophiolite, from the mantle section and the MTZ up to the crustal high-level gabbros. They are recognized on the basis of clear crosscutting relationships with the Phase 1 units, and as such are most easily recognized where they cut the layered gabbros. The Phase 2 intrusions are subdivided here into three groups: (1) wehrlite bodies within the MTZ and overlying crustal gabbros that locally crosscut higher parts of the crustal sequence; (2) microgabbro dikes in the mantle section, MTZ, and layered gabbros; (3) Gabbro-tonalite (GT-) intrusions—intrusive sheets and larger complexes in which gabbroic and tonalitic rocks are intimately associated that intrude the MTZ and crustal section. These include the Late Intrusive Complexes of Lippard et al. (1986), large masses of gabbro and tonalite, with outcrop areas of more than 1 km<sup>2</sup>, which are considered examples of classic Phase 2. In the GT-intrusions, the gabbroic lithologies are referred to as GT-gabbros and the felsic lithologies as GT-tonalites.

#### 3.1. Phase 2 Wehrlite Intrusions

The MTZ is a complex zone between the mantle and the crust, which comprises varying quantities of dunite, wehrlite, pyroxenite, and gabbro, and passes gradationally upward into layered gabbro. In Oman, the classic outcrops of the MTZ in the southernmost Semail and Wadi Tayin blocks (e.g., around Maqsad; Abily & Ceuleneer, 2013; Nicolle et al., 2016) comprise largely dunite and gabbro and have typically been attributed entirely to Phase 1, whereas further north in the ophiolite wehrlite (attributed to Phase 2) is more abundant (Goodenough et al., 2010). Recent work has identified mineral assemblages that indicate the presence of hydrous melts in the MTZ of the Maqsad area, but this has been attributed to the introduction of hydrothermal fluids (Rospabé et al., 2017). In the Maqsad area, the upper parts of the MTZ and layered gabbros are intruded by thin (few centimeters) sills and thicker sheets and lenses of Phase 2 wehrlites. In the ophiolite blocks north-west of the Semail Gap, the mantle section and MTZ contain abundant wehrlitic intrusions that are ascribed to Phase 2. At Somrah in the Semail Block, well-layered gabbros are cut by rare wehrlite sheets.

#### 3.2. Phase 2 Microgabbro Intrusions

Phase 2 gabbro intrusions within the mantle section are typically represented by microgabbro and pegmatitic dikes, up to 2.5 m wide, which have sharp contacts and crosscut fabrics in the mantle rocks. Higher up, in

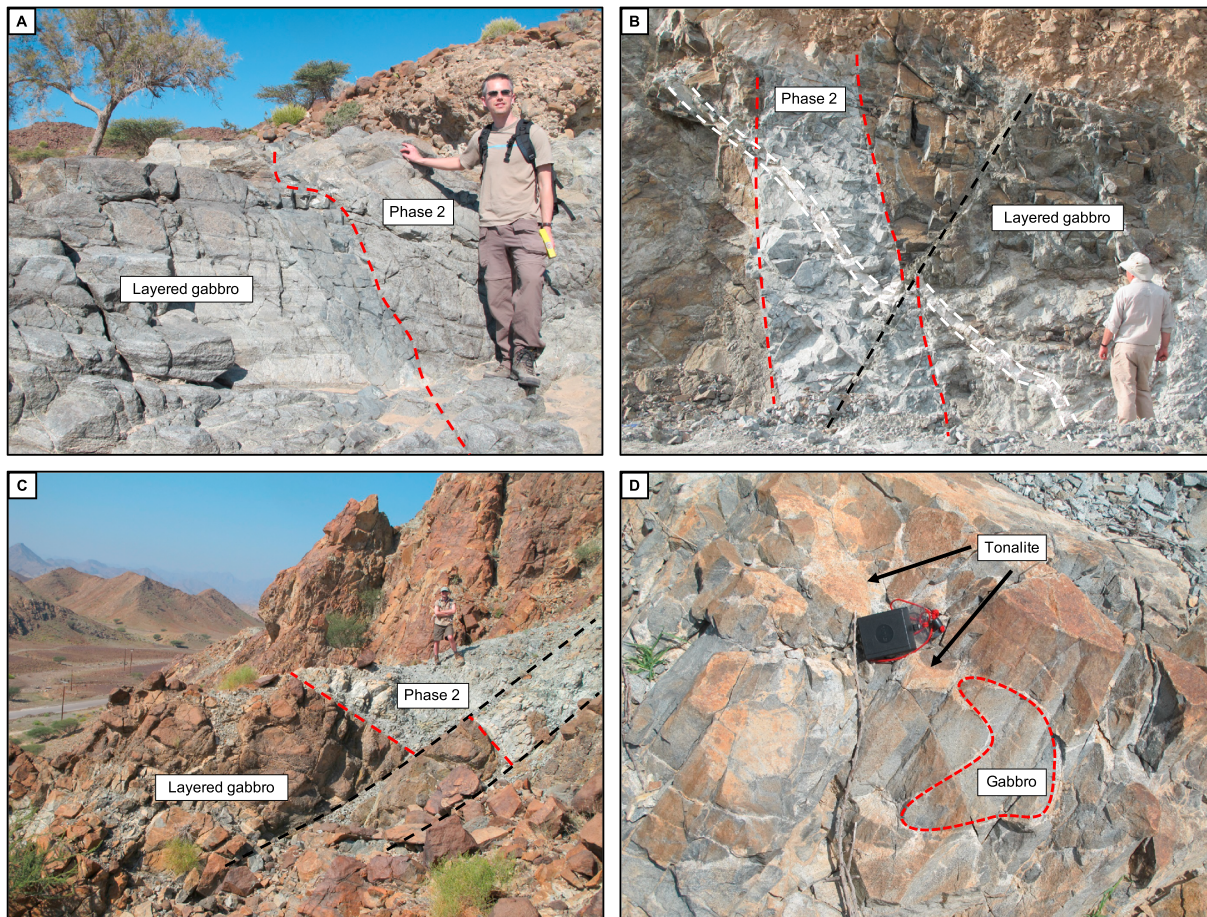


**Figure 2.** Field relations of Phase 2 intrusions in the Oman-United Arab Emirates ophiolite. (a) Microgabbro dike cutting layered gabbro at Somrah. (b) Layered gabbro cut by sheet of Phase 2 gabbro (red) in Wadi Wuqbah, which is in turn cut by a vein of tonalite (white), the whole is offset by a late fault. (c) Gray-weathering Phase 2 microgabbros with tonalitic veins intrude very coarse, weakly layered Phase 1 melagabbros in Wadi Haymilliah. (d) Magma mingling textures in the Jebel Shaykh intrusion. Gabbros are darkish gray and form irregular blebs. Tonalites are white with reddish weathering.

the MTZ and crustal section, microgabbro dikes up to 2 m thick are common (Figure 2a). These are attributed to Phase 2 where they clearly crosscut the Phase 1 ophiolite stratigraphy, including cutting wehrlite intrusions. In the latter they are sharply bounded and can be up to 1.5 m across.

### 3.3. Phase 2 GT-Intrusions

The GT-intrusions are common in most of the ophiolite blocks north-west of the Semail Gap and are characterized by clear evidence of mingling between basaltic and tonalitic magmas. These intrusions cut all levels of the MTZ and crustal section and vary from approximately 1 m wide sheets to the large Late Intrusive Complexes described by Lippard et al. (1986). Good examples occur in Wadi Wuqbah where the MTZ and layered gabbros are transected by abundant late, crosscutting sheets of Phase 2 gabbro and tonalite, up to 10 m thick (Figure 2b). Within these sheets the tonalitic lithology varies from irregular “blebs,” indicating magma mingling, to crosscutting veins. Similar intrusions occur along much of the length of the ophiolite, including the northern blocks in the UAE, where they are considered as part of the Fujairah facies of Phase 2 (Goodenough et al., 2010). They have been documented at shallower crustal levels such as the high-level gabbros in Wadi Haymilliah where they are up to a few meters in thickness (Figure 2c). An example of a larger GT-intrusion is the Jebel Shaykh intrusion in the Fizzh block (Figure 1), which occurs at the contact between the sheeted dikes and the underlying gabbro and is several hundred meters across. It comprises gabbro, microgabbro, and tonalite that are intimately associated with evidence of magma mingling (Figure 2d).

## 4. Methods

### 4.1. Sampling and Analysis

Fieldwork in Oman in January 2014 focused on sampling of Phase 2 intrusions across the Fizh, Sarami, Wuqbah, Haylayn, Rustaq, Semail, and Wadi Tayin Blocks (Figure 1). Twenty-six samples of Phase 2 intrusions have been collected along the length of the Omani part of ophiolite (Data Set S1). For comparison, 12 additional samples of typical Phase 2 GT-intrusions were collected from localities in the UAE (Data Set S1), as described by Goodenough et al. (2010). The Sheeted Dike Complex was sampled in the Wadi Tayin block to provide Phase 1 reference material for geochemical comparison (10 samples; Data Set S1). The sampled Phase 1 intrusions are all microgabbro dikes that are clearly part of the local Sheeted Dike Complex with chilled margins on one or both sides. Sample groups of closely spaced Phase 1 dikes were taken in two separate locations 20 km apart.

Where samples contain two mingled magmatic phases, the samples were carefully cut to separate the two. Weathered surfaces were removed with a table saw and samples were washed with distilled water in an ultrasonic bath before further sample handling. Major element, trace element, and Sr-Nd-Hf isotope analysis of the Omani samples was carried out at the Vrije Universiteit Amsterdam following the procedures outlined in Klaver et al. (2018) incorporating methods of Eggins et al. (1997) and Griselein et al. (2001). The UAE samples were prepared and analyzed at the British Geological Survey laboratories in Keyworth, Nottingham, following procedures outlined in Munker et al. (2001) and Nowell and Parrish (2001). Prior to digestion, powdered samples were subjected to hydrochloric acid leaching (following a method adapted from Nobre Silva et al., 2010) to remove the effects of possible low-temperature and hydrothermal alteration. More detailed information on sample treatment, analysis, and quality of the data for both sample groups are given in the online supporting information.

Plagioclase was separated at the Vrije Universiteit Amsterdam for two selected Phase 1 layered gabbros (from samples reported in Jansen et al., 2018; Data Set S1) and four Phase 2 intrusions (this study; Data Set S1) using conventional heavy liquid techniques and handpicked for absence of alteration and purity. Exceedingly fresh plagioclase separates ( $\pm 20$  mg) containing an estimated 3–5 ng Pb were digested in HF-HNO<sub>3</sub> at 140 °C and subsequently processed for Pb isotope analysis following the method of Klaver, Smeets, et al. (2016). Instrumental mass fractionation was corrected for with the use of a <sup>207</sup>Pb-<sup>204</sup>Pb double spike and <sup>204</sup>Pb was collected in a Faraday cup connected to a 10<sup>13</sup> Ω amplifier feedback resistor for the unspiked analysis. Further details and results for reference materials are given in the online supporting information.

### 4.2. MELTS Modeling

Liquid lines of descent were modeled following a modified method of MacLeod et al. (2013) using the 1.1.0 version of MELTS that includes H<sub>2</sub>O-CO<sub>2</sub> mixed fluid saturation models (Ghiorso & Gualda, 2015). The amount of water was varied between 0% and 4%, pressure was fixed at 2 kbar, which was defined as “shallow” fractionation at intracrustal depth and the total oxidation state was set at the QFM buffer. An experimental MORB parental melt composition from Kinzler and Grove (1993) was selected as the starting composition but with lowered titanium content to match the inferred parental melt of the ophiolite (MacLeod et al., 2013).

## 5. Results

### 5.1. Petrography

#### 5.1.1. Phase 1 Sheeted Dikes

The Phase 1 sheeted dike complex samples are equigranular to porphyritic, medium to fine-grained plagioclase-phyric microgabbros containing plagioclase (40–60%), and either clinopyroxene (20–30%) or amphibole (15–30%). A few samples contain large amounts of oxides (up to 30%) that appear to be primary magmatic phases due to their euhedral habit (Data Set S2). These observations contrast with the petrographic descriptions of Lippard et al. (1986) who noted only small amounts of iron oxides (<5%); this could suggest local variations in Phase 1 modal compositions.

#### 5.1.2. Phase 2 Wehrlites

The Phase 2 wehrlite samples contain poikilitic subhedral clinopyroxene enclosing large (up to 2 cm) subhedral to euhedral, commonly highly serpentinized olivine. Clinopyroxene shows variable amounts of

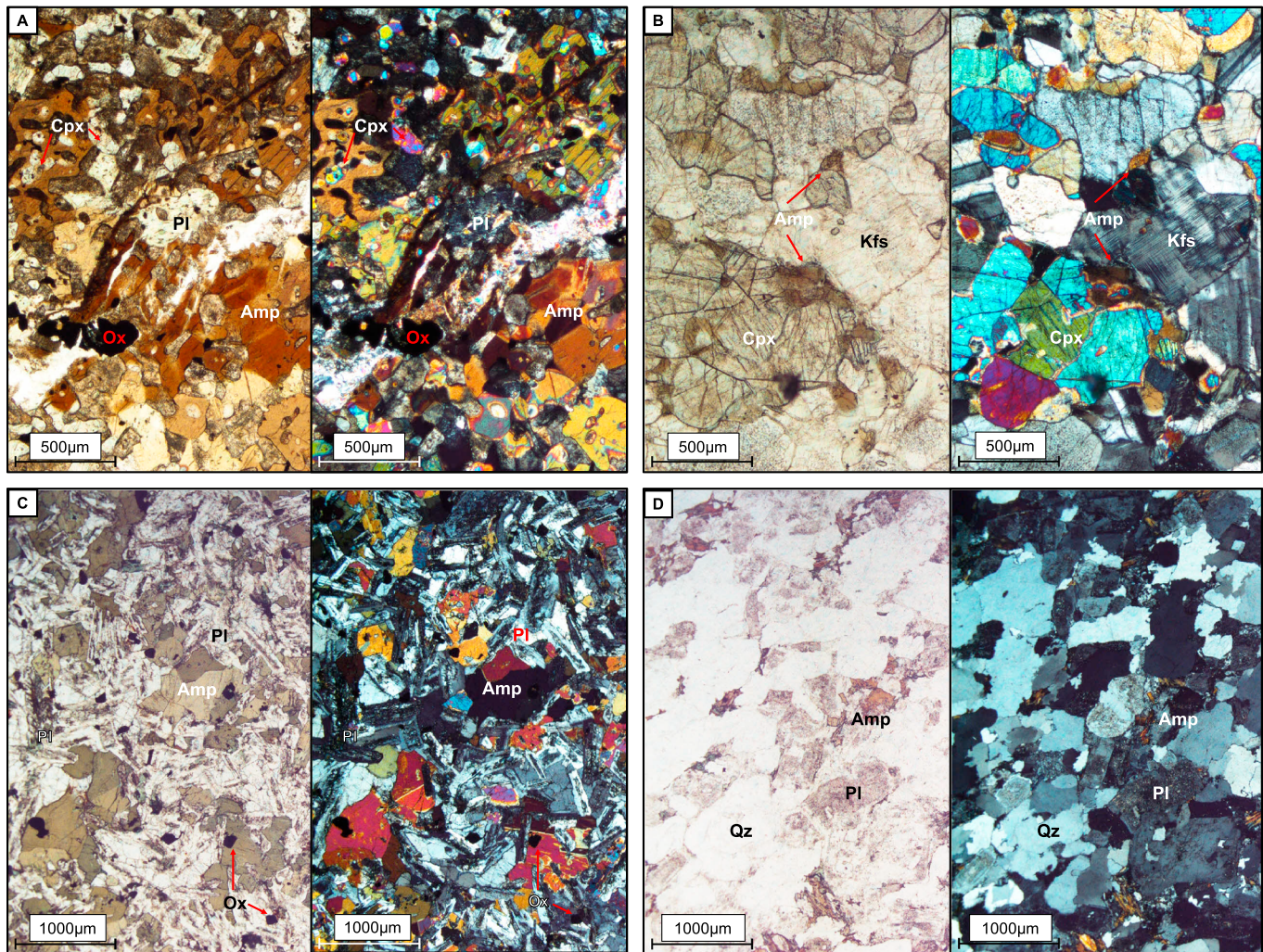


**Figure 3.** Representative thin sections of Phase 2 intrusions in PPL (left) and XPL (right). (a) Microgabbro dike Om/14/01 found crosscutting mantle harzburgites in Wadi Abyad. Note the pervasive brown amphiboles poikilitically enclosing clinopyroxene and plagioclase. (b) Microgabbro Om/14/03 in Wadi Abyad, note the presence of K-feldspar and brown amphibole at the rims of clinopyroxenes. (c) GT-gabbro Om/14/22 near Rustaq, note the more greenish coloration due to the more pervasive alteration typical of the stratigraphically higher samples. (d) GT-tonalite Om/14/34 in Wadi Wuqbah. Note the zoning and saussuritization of some plagioclase and the interstitial brown amphibole. Mineral abbreviations from Whitney and Evans (2010).

alteration, being locally highly altered to amphibole, chlorite, and possibly clinozoisite. Interstitial phases, where present, include plagioclase (5–15%) and brown amphibole (generally <5% with one sample having close to 10%). Subhedral to euhedral opaque mineral phases ( $\leq 1\%$ ) occur as inclusions in olivine as well as being associated with green alteration phases. The textures in the Phase 2 wehrlites suggest a crystallization sequence of olivine-clinopyroxene-plagioclase (Goodenough et al., 2010), and the presence of accumulated olivine enclosed within poikilitic clinopyroxene suggests that the composition of these rocks has been affected by cumulate processes.

### 5.1.3. Phase 2 Microgabbro Intrusions

The Phase 2 microgabbros contain 20–50% plagioclase, with the exception of one amphibole-rich, highly altered sample containing <5% plagioclase (Data Set S2). Plagioclase forms euhedral laths and/or anhedral blebs that vary from <0.1 to 2 mm, typically with low-temperature alteration to saussurite. Clinopyroxene is generally subhedral to anhedral where fresh but records evidence of extensive replacement by amphibole. Amphibole occurs throughout the sample group, commonly 30–50% of total mineral content. Subhedral to anhedral brown amphibole occur as individual crystals, representing a later magmatic phase (Figure 3a), or in rims surrounding and replacing clinopyroxene (Figure 3b). Dark to light green

amphibole is also present, and commonly has fibrous or blebby textures that indicate they are associated with hydrothermal alteration (Goodenough et al., 2010). Oxide phases are ubiquitous, varying from a subhedral to euhedral magmatic phase (up to 10% of total mineral content), to intergrowths with alteration phases such as green amphibole and/or chlorite. Chlorite is rare but where present forms small anhedral blebs (<0.5 mm). Clinzoisite has only been observed in an alteration vein in one sample. One microgabbro was found to contain subhedral grains of K-feldspar ( $\ll 1\%$ ; up to 1 mm; Figure 3b). The relationship between clinopyroxene and plagioclase is commonly ambiguous in the microgabbros, suggesting crystallization of the magma under conditions that to some extent favor clinopyroxene before plagioclase.

#### 5.1.4. GT-Intrusions

The GT-gabbros have a similar mineralogy to the Phase 2 microgabbro dikes, although they generally contain more plagioclase (approximately 50%; Figure 3c). The GT-gabbros are also largely microgabbroic, but we use the term GT-gabbro to ensure clarity throughout the text. Plagioclase crystals are typically subhedral to euhedral, forming laths (0.1–0.5 mm) and/or larger tabular crystals (up to 2 mm); the latter has less signs of low-temperature alteration. Fresh clinopyroxene is rare, forming subhedral to anhedral crystals (up to 1 mm), but in many samples is pervasively altered to pale green amphibole (actinolite). Brown amphibole is also present, though is only observed around the rims of green amphibole or clinopyroxene (Figure 3c). Oxide phases form subhedral to anhedral crystals (5–10%; up to 0.2 mm; Figure 3c) or may be intergrown with alteration phases. In contrast to the microgabbros, the GT-gabbros can contain small amounts of quartz (interstitial, up to 5%).

The GT-tonalites are medium- to coarse-grained and tonalitic in composition with typically up to 40% (rarely 50%) quartz and varying quantities of plagioclase (50–90%). Magmatic clinopyroxene and amphibole are locally present (<15%), typically interstitial, and are highly altered to chlorite and/or epidote. Zoning of plagioclase is generally rare (documented in a single sample; Figure 3d). At the thin-section scale, the GT-gabbro and GT-tonalite rock types are distinct with relatively sharp contacts, but evidence of gradational compositions is observed with the presence of quartz in some GT-gabbros.

## 5.2. Geochemistry

### 5.2.1. Whole Rock Elemental Compositions

The pervasive alteration observed in the petrography could have potentially compromised whole rock compositions of mobile elements (e.g., Na, K, Ba, U, and Sr). Correlation of MgO, Al<sub>2</sub>O<sub>3</sub>, SiO<sub>2</sub>, and Na<sub>2</sub>O with compositional variations in TiO<sub>2</sub> (Figures 4 and S1; Data Set S1), an element that is considered immobile during alteration processes (e.g., Staudigel et al., 1996), suggests that variation in these elements may be largely unaffected by alteration. K<sub>2</sub>O and CaO do show scatter (Figures 4 and S1; Data Set S1), implying that they could have been remobilized during alteration, however, K<sub>2</sub>O only varies between 0 and 0.6 wt% (with the exception of one GT-tonalite extending to 1.6 wt%), and thus does not cause large variations on the TAS diagram. Moreover, with the exception of the wehrlites, the samples have a loss on ignition (LOI) of <3 wt%, significantly lower than that observed in pervasively altered samples (e.g., Einaudi et al., 2000; up to 8 wt%).

#### 5.2.1.1. Phase 1 Samples

Phase 1 magmatism documented in the literature has large compositional variations (Figure 4), varying from gabbros with low total alkali content, to alkali-rich monzodiorites and more evolved diorites (Figure 5a). The Phase 1 samples in this study plot within this range (Figure 4) and are characterized by relatively high Na<sub>2</sub>O, K<sub>2</sub>O, and TiO<sub>2</sub>, and low CaO and LOI (Figure 4). They plot toward the more evolved variants of subalkaline to mildly alkaline gabbroic to monzodioritic compositions (Figure 5a) yet have FeO\*/MgO more comparable to tholeiitic compositions (Figure 5b). The MELTS liquid lines of descent for TiO<sub>2</sub> and Al<sub>2</sub>O<sub>3</sub> suggest Phase 1 contained between 0.1 and 1 wt% H<sub>2</sub>O (Figure 6), which is in agreement with MacLeod et al. (2013). N-MORB-normalized trace element diagrams (Figure 7) demonstrate that our Phase 1 reference samples are generally MORB-like and broadly comparable to average Phase 1 literature compositions (Godard et al., 2006) but that they differ in having Rb, Ba, Th, and Sr values that are notably higher (up to 1 order of magnitude) and small positive anomalies of Zr and Hf (Figure 7).

#### 5.2.1.2. Phase 2 Samples

The Phase 2 wehrlites are ultramafic rocks with low total alkalis (<1 wt%) and SiO<sub>2</sub> (<45 wt%) contents (Figure 4). They have the highest observed MgO and LOI contents of all sample groups but are the lowest in most other major elements with the exception of CaO and FeO\*, which is comparable to that of Phase



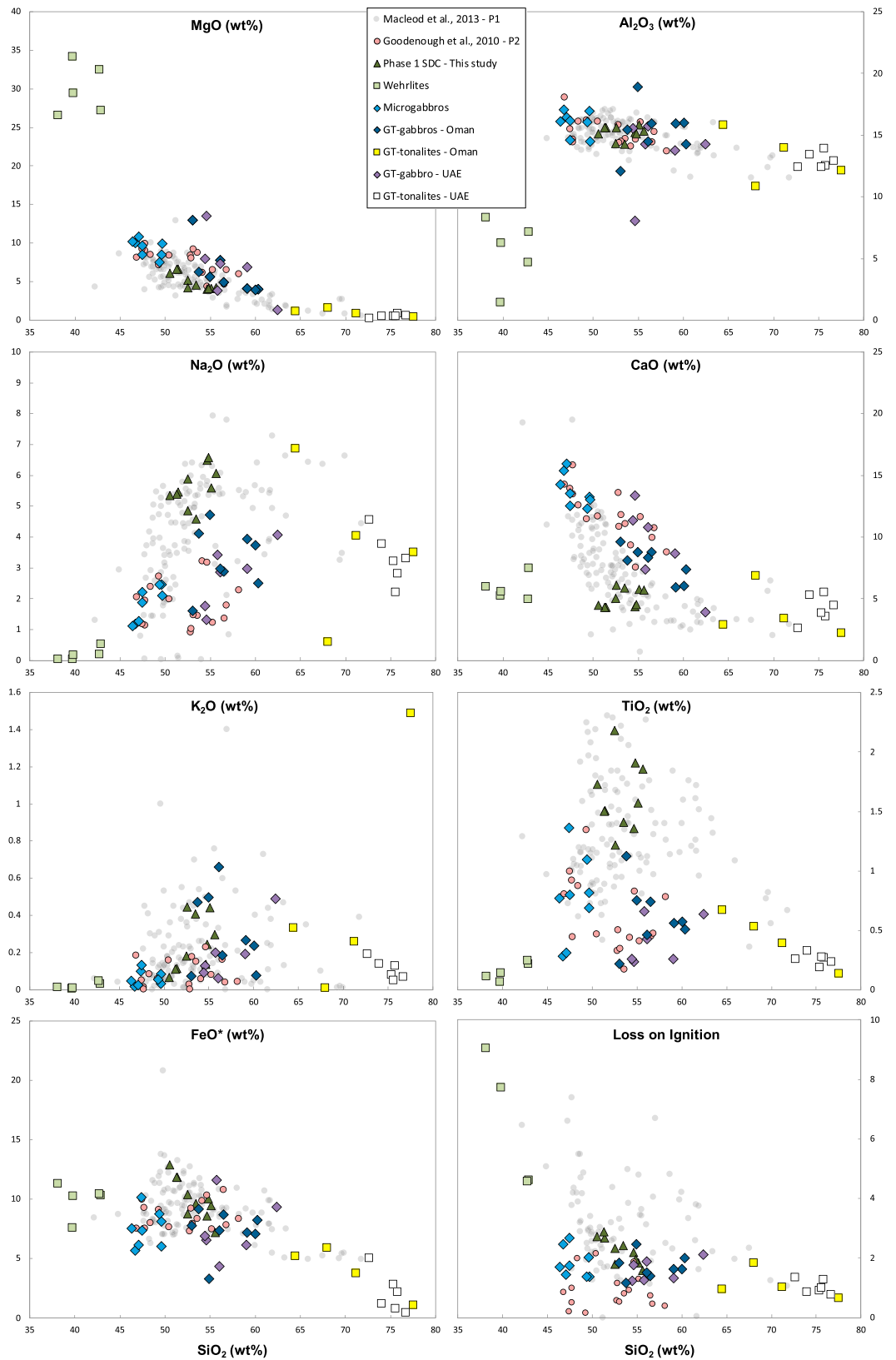


**Figure 4.** Major element compositions plotted against  $\text{SiO}_2$  (wt%) with all Fe expressed as total ferric Fe ( $\text{FeO}^*$ ). Data sets from MacLeod et al. (2013) and Goodenough et al. (2010) are used as reference samples for Phase 1 and Phase 2, respectively. SDC = Sheeted Dike Complex; GT = Gabbro-tonalite; UAE = United Arab Emirates.

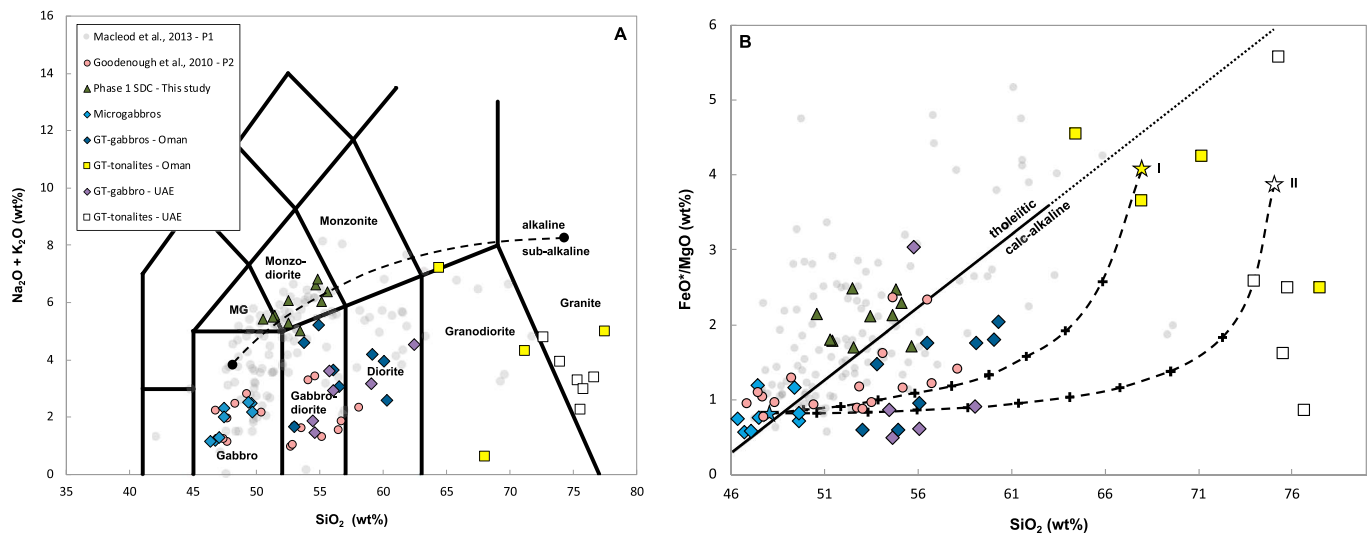


**Figure 5.** (a) TAS diagram after Le Maitre et al., 2005; alkaline/subalkaline line from Irvine and Baragar (1971). MG = Monzogabbro. (b) FeO\*/MgO plotted versus SiO<sub>2</sub>. Tholeiitic versus calc-alkaline line from Miyashiro (1974); the original line did not extend further than 65 wt% SiO<sub>2</sub> and dashed line represents linear extrapolation. Mixing lines are calculated between a mafic end-member and (I) Averaged GT-tonalite—Oman composition and (II) Averaged GT-tonalite—UAE composition. Each cross represents 10% mixing. SDC = Sheeted Dike Complex; GT = Gabbro-tonalite; UAE = United Arab Emirates.

1 and the GT-tonalites (Figure 4; Data Set S1). Moreover, they are significantly depleted in trace element composition with REE contents averaging 0.1 times N-MORB, but with normalized values as low as 0.01 for Nb, while showing a slight positive Eu anomaly (Figure S2, Data Set S1).

The most primitive of the gabbroic Phase 2 samples are the microgabbro dikes, which have gabbro to gabbroic diorite compositions (Figure 5a) recording lower SiO<sub>2</sub> (45–50 wt%) and lower total alkali content (1–3 wt%) when compared to the Phase 1 dikes. These microgabbro dikes have relatively high CaO and MgO contents, notably higher than both GT-gabbros and Phase 1 samples (Figure 4) consequently resulting in lower FeO\*/MgO ratios (Figure 5b). The GT-gabbros contain between 55 and 60 wt% SiO<sub>2</sub> with total alkalis between 2 and 4 wt% (Figure 5a) extending into the diorite field on the TAS diagram (Figure 5a). They have generally lower MgO and similar FeO\* contents compared to the microgabbros (Figure 4) resulting in higher FeO\*/MgO (Figure 5b).

At any given SiO<sub>2</sub> content, Phase 2 gabbros have higher CaO contents and generally lower Na<sub>2</sub>O contents and similar Al<sub>2</sub>O<sub>3</sub> than Phase 1 (Figures 4 and 6b). Most notable is the characteristically low TiO<sub>2</sub> content of all Phase 2 gabbros with most samples below 1 wt% and ~50% of the data below 0.5 wt% (Figures 4 and 6a). The Phase 2 microgabbro dikes appear to contain on average more TiO<sub>2</sub> than the GT-gabbros with two samples having >1 wt% TiO<sub>2</sub> (Figures 4 and 6a). The liquid lines of descent for TiO<sub>2</sub> suggest in excess of 4 wt% water, compared to the 0.1–0.5 wt% shown in the majority of Al<sub>2</sub>O<sub>3</sub> content (Figure 6; only one sample plots on the 4 wt% liquid lines of descent). Neither group of gabbroic rocks has LOI >3 wt%. Compared to the Phase 1 reference samples and literature data (Godard et al., 2006; Figure 7) both Phase 2 gabbro groups typically record depletion in the high field strength elements, most being below N-MORB values but with an overall flat N-MORB-normalized REE pattern, averaging around 0.5 times N-MORB. A generally small negative Eu anomaly and relative depletion in Y content compared to Yb and Lu is observed (Figure 7). The GT-gabbros have notable enrichment in the large ion lithophile elements (LILE; Rb, Ba, U, and Sr), whereas the microgabbros record relative depletion in these elements. The relatively high Ba and Sr content compared to Th and Nd, respectively, highlight the enrichment in 2+ cations of the samples (Figure 7). While the GT-gabbros are strongly comparable to average Phase 2 compositions (Goodenough et al., 2010) the Omani GT-gabbros record weak positive Zr and Hf anomalies as opposed to the weak negative anomalies seen in the UAE samples and previously published Phase 2 data (Figure 7; Goodenough et al., 2010).

The GT-tonalites plot in the granodioritic to granitic fields on the TAS diagram, with often lower total alkalis than their associated gabbros (Figure 5a) but similar TiO<sub>2</sub> content and LOI (Figures 4 and 6a). They have the

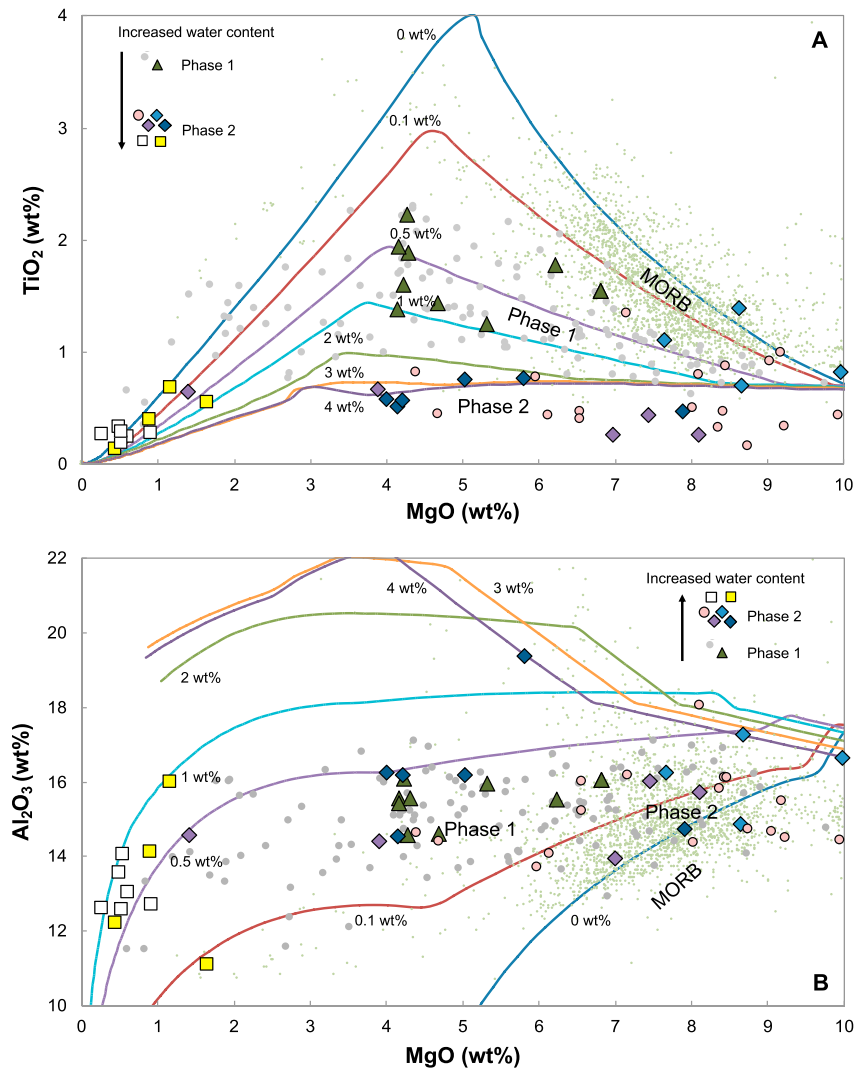


**Figure 6.** Melts liquid lines of descent modeled for (a)  $\text{TiO}_2$  (anhydrous) and (b)  $\text{Al}_2\text{O}_3$  (anhydrous). Arrows indicate increased water content. MORB data compilation from the PetDB database ( $n = 2420$ ; Lehnert et al., 2000; Data Set S3; see section 4 for further details). Key as in Figure 4. MORB = mid-ocean ridge basalts.

highest  $\text{SiO}_2$  content of all sample groups (up to  $\sim 77$  wt%  $\text{SiO}_2$ ). The GT-tonalites sampled in the UAE have typically more clustered compositions, whereas the Omani samples record larger variations (Figure 4). Mixing lines calculated between a mafic end-member and the GT-tonalites establish that the GT-gabbros plot close to these trends (Figure 5b), implying a clear relationship between the two. Both MELTS liquid lines of descent for  $\text{TiO}_2$  and  $\text{Al}_2\text{O}_3$  suggest  $\text{H}_2\text{O}$  content to have been between 0.5 and 1 wt%. The GT-tonalites have N-MORB normalized trace element patterns with a similar shape to those of average Phase 2 compositions but generally more enriched, being closer to N-MORB values, with distinct enrichment in Zr and Hf (up to 10 times N-MORB in one sample). With the exception of two Omani samples a negative Eu anomaly is observed but all GT-tonalites record a similar relative depletion in Y content as the GT-gabbros. GT-gabbro and GT-tonalite samples from the UAE and Oman have overlapping patterns, supporting their origin as part of the same magmatic suite.

### 5.2.2. Incompatible Element Ratios

Incompatible element ratios such as La/Yb, Th/Yb, and Nb/Yb have been shown to distinguish between hydrous and anhydrous melting, while also being less affected by alteration (e.g., Einaudi et al., 2000; Godard et al., 2006; Hastie et al., 2007; Müller et al., 2017; Pearce, 2008, 2014). These ratios emphasize the difference between Phase 1 and Phase 2 magmatic phases. Phase 2 documents greater depletion of LREE

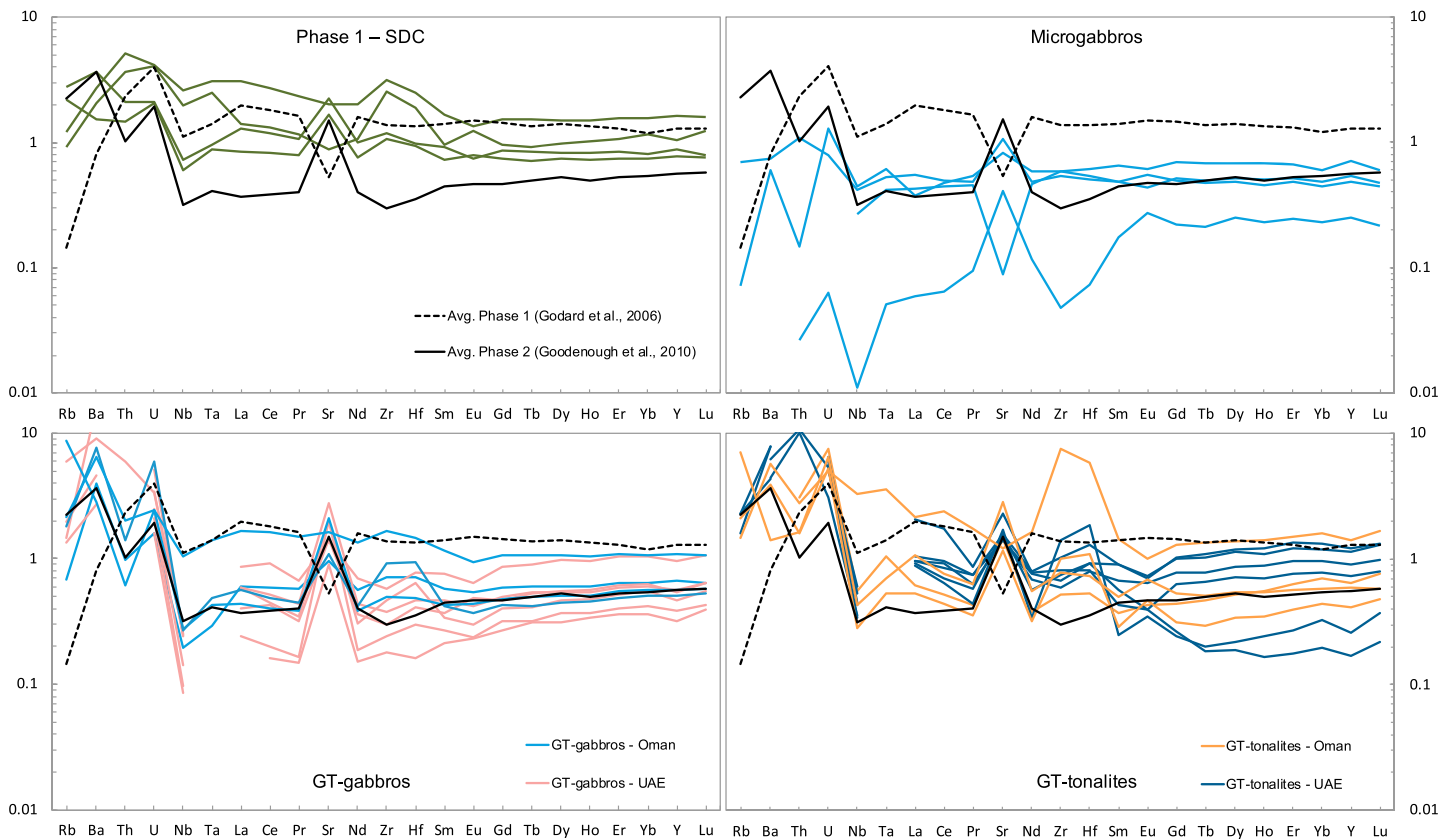


**Figure 7.** Normal mid-ocean ridge basalts normalized trace element diagrams. Normalization values and element sequence after Sun and McDonough (1989). Average Phase 1 and Lasail lava compositions from Godard et al., 2006. Average Phase 2 composition from Goodenough et al., 2010. SDC = Sheeted Dike Complex; GT = Gabbro-tonalite; UAE = United Arab Emirates.

((La/Yb)<sub>n<sub>chon</sub></sub> < 0.8) with higher MgO content (4–10 wt% MgO) compared to a relatively less LREE-depleted signature in Phase 1 ((La/Yb)<sub>n<sub>chon</sub></sub> = 0.8–1.2 at 3–5 wt% MgO; Figure 8a). The microgabbros, GT-gabbros, GT-tonalites, and Phase 1 samples all have Th enrichment compared to Nb (Figure 8b). Phase 1 samples are only slightly displaced from the MORB-OIB array (Pearce, 2008; Th/Yb ~0.1 and Nb/Yb ~1), whereas the Phase 2 samples are increasingly displaced (Figure 8b; with varying Th/Yb ratios between 0.04 and 2 at Nb/Yb between 0.2 and 1.6), with the UAE samples having the largest overall enrichment in Th compared to Yb. The GT-tonalites document the highest Th/Yb ratios (0.5–1.2) observed in our Phase 2 samples, whereas the wehrlites generally record the lowest, plotting within the MORB-OIB array (Figure 8b).

### 5.2.3. Isotopic Compositions

Representative bulk-rock samples were analyzed for Sr, Nd, and Hf isotopes and are compared with hitherto unpublished isotope data for a subset of the UAE Phase 1 and Phase 2 samples presented by Goodenough et al. (2010; Figure 9; Data Set S1). All sample groups have been age corrected to initial values, assuming an age of 96 Ma for Phase 1 and 95 Ma for Phase 2 (Goodenough et al., 2010; Rioux et al., 2012, 2013; Warren et al., 2005). Phase 1 and Phase 2 samples overlap in isotopic composition with both recording a general positive correlation between <sup>143</sup>Nd/<sup>144</sup>Nd<sub>i</sub> (0.5127–0.5130; εNd<sub>i</sub> +7 – +9) and <sup>176</sup>Hf/<sup>177</sup>Hf<sub>i</sub> (0.28313–0.28320; εHf<sub>i</sub> +14.7 – +16.6). With the exception of five samples, Phase 1 and Phase 2 samples have initial isotopic compositions within error of Indian MORB at 96 Ma (Figure 9a). Strontium isotopes show variations (<sup>87</sup>Sr/<sup>86</sup>Sr<sub>i</sub> 0.7030–0.7045; with one UAE sample extending to 0.7058) at constant Nd compositions (<sup>143</sup>Nd/<sup>144</sup>Nd<sub>i</sub> 0.5127–0.5130; Figure 9b). These <sup>87</sup>Sr/<sup>86</sup>Sr<sub>i</sub> ratios are considered high and, when comparing these values to the hydrothermally altered samples of Godard et al. (2006; Figure 9b) likely indicate a nonprimary isotopic signal (e.g., Godard et al., 2006; Kawahata et al., 2001).

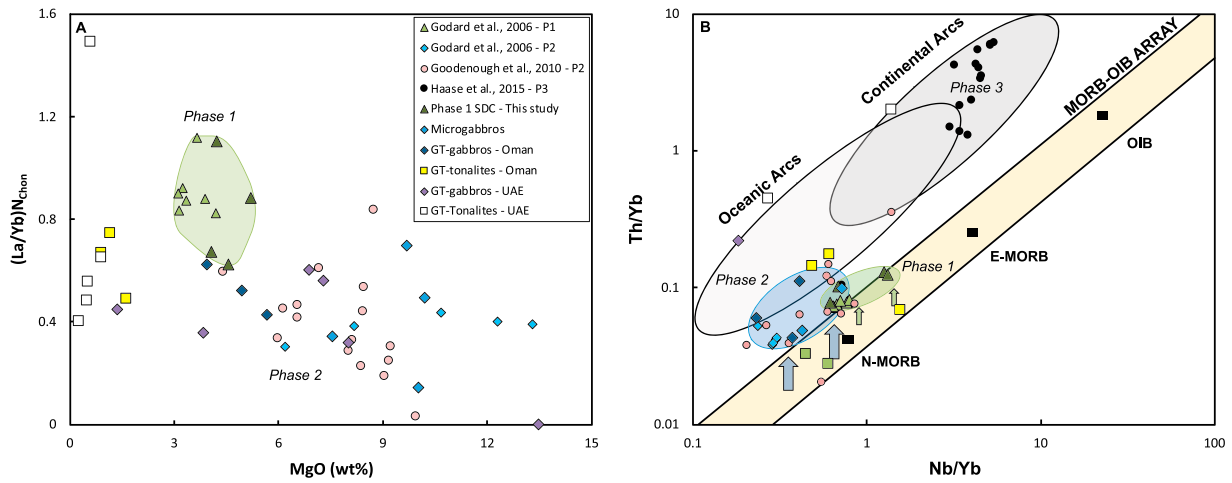


**Figure 8.** (a) Chondrite normalized La/Yb values of samples and reference material versus MgO. Normalization values from Sun and McDonough (1989). Haase et al.'s (2015) Phase 3 data set extends to La/Yb values above 1.6 and has not been incorporated in this figure. (b) Influence of slab material examined through Th/Yb versus Nb/Yb. Fields from Pearce (2014). The green field represents Phase 1 data. The Phase 2 field encompasses the majority of Phase 2 data presented in this study, notice how the majority of Phase 2 literature data presented here falls within this field. SDC = Sheeted Dike Complex; GT = Gabbro-tonalite; UAE = United Arab Emirates; MORB = mid-ocean ridge basalts; N-MORB = normal MORB; E-MORB = enriched MORB; OIB = ocean island basalts.

Whole rock Pb isotope compositions suffer from large uncertainties introduced by the age correction and variable mobility of U, Th, and Pb and are hence not presented. In contrast, plagioclase can be used as a proxy for the initial Pb isotopic compositions. Age corrections are trivial as Pb is mildly incompatible, but U and Th are strongly excluded from the plagioclase structure (e.g., Bédard, 2006). The Phase 2 samples have variably more radiogenic <sup>206</sup>Pb/<sup>204</sup>Pb, <sup>207</sup>Pb/<sup>204</sup>Pb, and <sup>208</sup>Pb/<sup>204</sup>Pb compared to the Phase 1 samples and fall on a trend away from the Indian MORB array (Figure 10). A microgabbro and tonalite from the same outcrop in Wadi Haymilliah have indistinguishable plagioclase Pb isotope compositions.

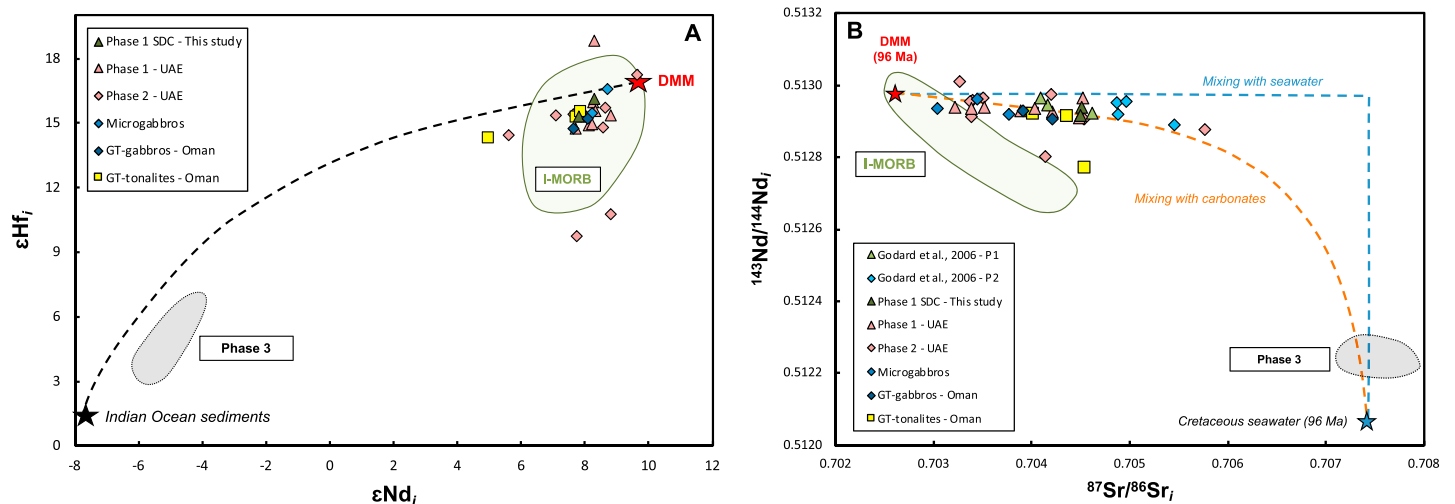


**Figure 9.** Based on the apparent source depletion observed in the (La/Yb)<sub>n<sub>chon</sub></sub> ratios, mixing lines are calculated between a DMM source from Workman and Hart (2005) and varying components. I-MORB data set from the PetDB database ( $n = 278$ ; Lehnert et al., 2000; compiled by Jansen et al., 2018). Phase 3 from Haase et al., 2015. (a) εHf<sub>i</sub> versus εNd<sub>i</sub> record small inclination toward mixing with sediments, mixing line calculated between DMM and Indian Ocean sediment (Othman et al., 1989; White et al., 1986). (b) Initial isotopic compositions of Nd plotted against Sr. Mixing lines calculated between DMM and a seawater end-member (Bralower et al., 1997; McArthur et al., 2012; Stille et al., 1996) at 96 Ma with varying contributions of trench carbonates (Plank & Langmuir, 1998). Phase 1, I-MORB, seawater, and DMM have been age corrected to 96 Ma, Phase 2 has been age corrected to 95 Ma and represent initial values. Error bars are smaller than symbol size. SDC = Sheeted Dike Complex; GT = Gabbro-tonalite; UAE = United Arab Emirates; I-MORB = Indian mid-ocean ridge basalts; DMM = depleted MORB mantle.

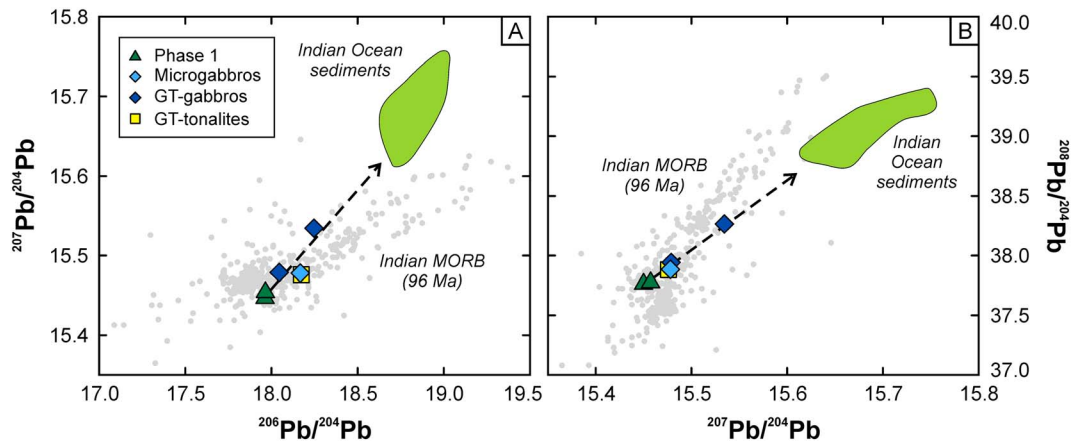


**Figure 10.** Pb isotope diagrams showing the (a)  $^{207}\text{Pb}/^{204}\text{Pb}$  versus  $^{206}\text{Pb}/^{204}\text{Pb}$  and (b)  $^{208}\text{Pb}/^{204}\text{Pb}$  versus  $^{207}\text{Pb}/^{204}\text{Pb}$  composition of plagioclase separated from the Phase 1 layered gabbros and Phase 2 samples. Phase 2 samples are offset from the Phase 1 layered gabbros toward an Indian Ocean sedimentary component (Othman et al., 1989). The trend defined by the samples is clearly at an angle compared to the Indian MORB array (age corrected to 96 Ma assuming depleted MORB mantle, Workman & Hart, 2005, U, Th, and Pb contents of the mantle source), suggesting it is unlikely to result from lateral variations in the Pb composition of the mantle but reflects the addition of a component derived from a subducting slab. Error bars are smaller than symbol size. GT = Gabbro-tonalite; MORB = mid-ocean ridge basalts.

## 6. Discussion

### 6.1. The Importance of Phase 2 Magmatism

The Oman-UAE ophiolite has been the subject of much debate relating to its geodynamic history and the importance, or lack thereof, of SSZ fluids and magmas in its genesis (Abily et al., 2011; Alabaster et al., 1982; Benoit et al., 1996, 1999; Bosch et al., 2004; Boudier et al., 2000; Ernewein et al., 1988; Godard et al., 2006; Goodenough et al., 2014; MacLeod et al., 2013; Nicolas & Boudier, 2015; Pearce et al., 1981). The recent grouping of the ophiolite's magmatic history in Phase 1 and Phase 2 by Goodenough et al. (2014) has helped to elucidate the complex geodynamic history of the ophiolite, but it is still commonly suggested that Phase 2 was of less significance in the southern blocks. Recently documented Phase 2 plagiogranites (Haase et al., 2016) and intrusions related to Phase 2 (Müller et al., 2017) in the southern part of the ophiolite indicate the more widespread nature of this phase of magmatism. Here we document additional Phase 2 rock types in the central and southern part of the ophiolite and conclude that this type of magmatism is present throughout the entire ophiolite. The recognition of ophiolite-wide, pre-remagnetization clockwise rotation of the ophiolite prior to obduction (Morris et al., 2016) agrees with this observation as it removes the need for complex tectonic models involving large differential rotations, which argues for more lateral consistency in magmatic sequences. Except for the Phase 2 wehrlite cumulates, the Phase 2 lithologies are typically fine to medium-grained and form relatively thin intrusive sheets. These lithologies are rich in plagioclase but only a few, more evolved, samples show a slight positive Eu anomaly that could indicate plagioclase accumulation (Figure 7). These observations and their similarities to rocks described in the literature (Goodenough et al., 2010, 2014; Haase et al., 2016) indicate that the Phase 2 gabbros and tonalites discussed here have not been significantly affected by crystal accumulation. This strongly suggests their geochemical composition to represent (near) original melt compositions (hydrothermal alteration notwithstanding). This allows us to use Phase 2 magmatism to draw more general conclusions about the geodynamic setting of the ophiolite.

### 6.2. The Extent of Hydrothermal Alteration

Alteration by seawater-derived fluids is a common problem in ophiolitic crustal rocks (Alabaster et al., 1982; Godard et al., 2006; Haase et al., 2016; Kawahata et al., 2001; Müller et al., 2017; Pearce et al., 1981). In this study clinopyroxene is widely replaced by green amphibole (actinolite), and chlorite, in association with epidote-group minerals and oxides (Data Set S2), most likely representing greenschist to lower amphibolite facies metamorphism (Haase et al., 2016). This is apparent in the wehrlitic samples, which record highly altered olivine and widespread replacement of clinopyroxene by alteration phases. These samples also document the highest observed LOI (up to 10%, Figure 4) and therefore likely record pervasive alteration. In

contrast the majority of the gabbroic and tonalitic samples show a correlation of major element variations with compositional variations in  $\text{TiO}_2$ , small variations in  $\text{K}_2\text{O}$ , consistent positive anomalies of fluid mobile elements (Ba, U, and Sr; Figure 7), and a typically low LOI (around 2 wt%, Figures 4 and S1; Data Set S1). When comparing these results to more heavily altered Omani samples (e.g., Einaudi et al., 2000, up to 8 wt% LOI) this suggests the geochemical variations in the gabbroic and tonalitic samples to record a less altered signal (see also Haase et al., 2016). Nonetheless, care is taken when interpreting the geochemical data and the focus is on immobile element variations.

### 6.3. Fluid Content of the Ophiolite Source

Changes in fluid content of a magma source can strongly affect magmatic compositions. The decoupling of total alkalis and  $\text{FeO}^*/\text{MgO}$  observed in both the Phase 1 and Phase 2 sample groups is related to changes in oxygen fugacity and  $\text{H}_2\text{O}$  contents (Arculus, 2003). Moreover, the petrographic observations in Phase 2 support early plagioclase suppression: most notably, interstitial plagioclases in some wehrlite cumulates strongly indicates clinopyroxene-before-plagioclase crystallization (Data Set S2, also see Boudier & Nicolas, 1995; Goodenough et al., 2010; Juteau et al., 1988, who described similar textures). This demonstrates a variation in fluid content between Phase 1 and Phase 2, with Phase 2 appearing to record more hydrous compositions.

This variation is quantified by modeling the liquid lines of descent for  $\text{TiO}_2$  and  $\text{Al}_2\text{O}_3$ . Variation in the  $\text{TiO}_2$  content of magmatic rock is mainly controlled by olivine, clinopyroxene, and plagioclase fractionation during the high-temperature part of the liquid line of descent (retention of  $\text{TiO}_2$ ), followed by fractionation of Fe-Ti-oxides at lower temperatures (MacLeod et al., 2013) and to a lesser extent by amphibole (removal of  $\text{TiO}_2$ ). Variation in  $\text{Al}_2\text{O}_3$  is mostly a function of plagioclase fractionation. The amount of clinopyroxene, amphibole, and plagioclase fractionation and the point of Fe-Ti-oxide saturation are controlled by water content (Davidson et al., 2007; Koepke et al., 2009; Langmuir et al., 1992; MacLeod et al., 2013; Sisson & Grove, 1993). MELTS modeling establishes that the differences in  $\text{TiO}_2$  and  $\text{Al}_2\text{O}_3$  between MORB, Phase 1, and Phase 2 magmatism can be explained by increased hydration of the source. Phase 2 gabbros (most notably the GT-gabbros) follow  $\text{TiO}_2$  liquid lines of descent as high as 4 wt %  $\text{H}_2\text{O}$  (Figure 6a). Interestingly, with the exception of one sample, the  $\text{Al}_2\text{O}_3$  data show water contents to be much lower, between 0.1 and 1 wt% (Figure 6b,  $\text{Al}_2\text{O}_3$ ; see also MacLeod et al., 2013; Müller et al., 2017), with no major difference in  $\text{Al}_2\text{O}_3$  contents between Phase 1 and Phase 2. These differences could be explained by the fractionation of additional minerals different from that predicted in the MELTS formulation (e.g., amphibole as this is not incorporated in the MELTS formulation). A more likely explanation, however, is that the GT-gabbros were formed by mixing of a low  $\text{TiO}_2$  mafic component (the microgabbros) and the GT-tonalites, which is also suggested by the mixing lines shown in Figure 5b and the presence of quartz in the Gt-gabbros (Data Set S2). Consequently, the MELTS results do not conclusively suggest Phase 2 to be more hydrated than Phase 1, but the fundamental observation is that both Phase 1 and Phase 2 of the Oman-UAE ophiolite clearly show more hydrated fractionation trends than anhydrous MORB (Figures 4–6).

### 6.4. Nature of the Phase 2 Source

In the context of a hydrated source for the Phase 2 magmatism, it is important to understand the origin of these fluids and the source they hydrated to determine the ophiolite's geodynamic history. To explain fluid addition in a MOR setting, hydrated low-pressure melting of an upwelling mantle diapir (Benoit et al., 1999; Nicolle et al., 2016; Rospabé et al., 2017) or hydrated melting of the inner margin of the magma chamber as a result of seawater penetration (Bosch et al., 2004; Boudier et al., 2000; Nicolas et al., 2003) have been proposed. In the case of the former, such intrusions are limited to the proximity of a mantle diapir and can only account for hydrated intrusions close to mantle upwelling zones (e.g., Maqsad; Benoit et al., 1999, or Mansah; Nicolle et al., 2016). These studies thus fail to reconcile the widespread distribution of Phase 2 documented in this and other studies (e.g., Haase et al., 2016; Müller et al., 2017). Moreover, mantle chromitites documented in the Maqsad area (Borisova et al., 2012; Rollinson, 2005; Rollinson & Adetunji, 2013) are interpreted as non-MORB-like podiform chromitites (Rollinson & Adetunji, 2013), questioning the MORB origin of the Maqsad diapir. In the case of seawater penetration, an important observation is that Phase 2 microgabbros have been documented below the Moho Transition Zone (MTZ) both in this study and in the north of the ophiolite (Goodenough et al., 2010). Explaining the widespread Phase 2 magmatism by

seawater penetration would then require large amounts of water to have infiltrated the crust at great depths across the length of the ophiolite. Such a scenario is considered unlikely. Taking all these points into consideration, we postulate that these studies can only account for localized hydrous melts and as such a hydrated mantle source for Phase 2 has to be considered.

The identical Hf and Nd isotopic composition (Figure 9a) of Phase 1 and Phase 2 establishes that they originated from the same source (see also Godard et al., 2006; Goodenough et al., 2010, 2014). The low La/Yb ratios in Phase 2 (Figure 8a) suggest that the mantle source was more depleted compared to Phase 1, yet identical Nd and Hf isotope composition imply that the enhanced depletion was a recent feature otherwise Phase 2 would have shown more radiogenic values. This is in agreement with Phase 2 being formed  $\pm 1$  Myr after the formation of the main crustal sequence (Rioux et al., 2012, 2013). In an anhydrous MORB melting system, Th and Nb, both highly incompatible elements, have similar behavior, resulting in a linear relationship between the Th/Yb and Nb/Yb (Figure 8b; Pearce, 2008, 2014). In contrast, in a hydrous arc-like setting Th and Nb become decoupled as fluid metasomatism of the mantle wedge is able to mobilize Th but not Nb (Elliott, 2003; Pearce, 2008). Both the Phase 1 and Phase 2 microgabbros, GT-gabbros and GT-tonalites are displaced from the MORB-OIB array (Figure 8), with the Phase 2 ratios extending to higher values of Th/Yb while having lower, more depleted Nb/Yb values. These Th/Yb values do not justify the addition of a slab-derived melt, as the addition of just a few permille of sediment would increase the Th/Yb content more significantly (Elliott, 2003; Klaver, Davies, & Vroon, 2016) as can be clearly observed in Phase 3, which is interpreted to represent a sediment-derived melt (Haase et al., 2015; Figure 8). The excess of 2+ cations in Phase 2 magmatism compared to Phase 1, however, is a tell-tale sign of a fluid dominated contribution from the slab (Elliott, 2003). The Th/Yb values observed in Phase 2 therefore likely indicate the addition of a slab-derived fluid while Nb/Yb highlight the need for a higher degree of melting of a previously depleted mantle source. This strongly suggests that Phase 2 had to be formed by fluid-assisted melting of the depleted mantle source but without a strong sediment melt input at that moment. The coupled  $\epsilon_{\text{Hf}}$  and  $\epsilon_{\text{Nd}}$  data of Phase 2 samples support this interpretation as they are mostly indistinguishable from Indian MORB and Phase 1 (Figure 9a), with only the most unradiogenic values potentially showing a small sediment or crustal input (Figure 9a). The addition of a sediment-derived melt would have recorded lower  $\epsilon_{\text{Hf}}$  and  $\epsilon_{\text{Nd}}$  ratios (e.g., Haase et al., 2015; Klaver, Davies, & Vroon, 2016; Nebel et al., 2011; Figure 9a) as can be observed in the Phase 3 samples that display much more crustal Nd-Hf isotope compositions (Haase et al., 2015). Phase 2 plagioclases do, however, record more radiogenic Pb isotope compositions compared to Phase 1 and define a trend toward Indian Ocean sediments (Figure 10). This Pb isotope trend is clearly at an angle compared to the Indian MORB array, indicating that it does not result from lateral mantle heterogeneity but reflects a recycled component from a subducting slab. The greater enrichment in Sr and Ba than Th, homogeneous Nd-Hf isotope compositions but more radiogenic Pb are consistent with a fluid component derived from sediments or altered oceanic crust rather than a sedimentary melt. Hence, we conclude that Phase 2 records a clear subducting slab-derived fluid signature, but with no evidence of a sediment melt having entered the system during formation of Phase 2. That said, the few samples that do plot toward sediment melt compositions could represent an even later stage intrusion more akin to the onset of Phase 3 magmatism (Haase et al., 2015, 2016; Figures 8–10). Following these conclusions, we suggest the following temporal evolution of the first two phases of magmatism of the Oman-UAE ophiolite: Phase 1 compositions are consistent with moist melting above an incipient subduction zone (as proposed by MacLeod et al., 2013), while Phase 2 records an increased subduction input due to increased fluid metasomatism of the mantle wedge causing further melting of an increasingly depleted mantle source.

### 6.5. The Role of Primary Amphibole Fractionation

The Phase 2 gabbros, wehrlites, and tonalites are characterized by the presence of brown amphibole and iron oxides (Figure 3). Petrographical evidence indicates that these represent primary magmatic phases best observed in the stratigraphically lower microgabbros. Paired with the inferred arc-like conditions in the previous section, it is necessary to consider the role of amphibole during differentiation of the Phase 2 magmatic series as it represents a major fractionating phase in hydrous (arc) settings (e.g., Alonso-Perez et al., 2009; Cawthorn & O'hara, 1976; Melekhova et al., 2015; Nandedkar et al., 2014; Sisson & Grove, 1993).

Middle REE (MREE) fractionation is a characteristic of amphibole involvement in the genesis of a magma (Davidson et al., 2007; Klaver, Carey, et al., 2016). Amphibole preferentially incorporates MREEs over



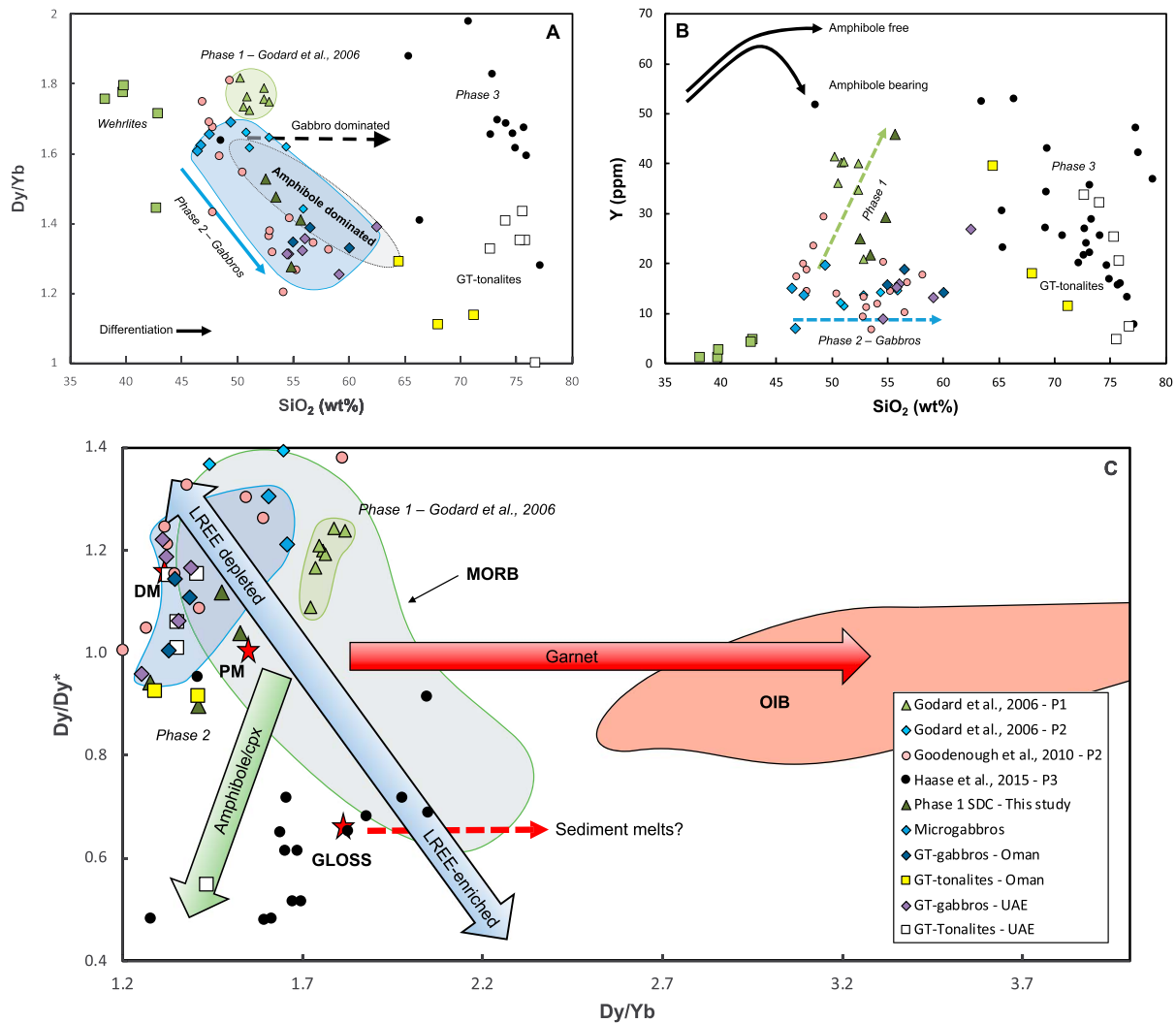


**Figure 11.** (a) Dy/Yb versus SiO<sub>2</sub>, fractionation trends from Davidson et al. (2007). Note the similarities to data from the Lesser Antilles. (b) Yttrium versus SiO<sub>2</sub>, Showing the relative low amounts of Y in Phase 2 magmatism compared to Phase 1, indicative of the influence of amphibole (Davidson et al., 2007; Klaver, Carey, et al., 2016). Fractional crystallization vectors from Klaver, Carey, et al. (2016). (c) Dy/Dy\* versus Dy/Yb following the methodology of Davidson et al. (2012). DM = Depleted Mantle; PM = Primitive Mantle; GT = Gabbro-tonalite; LREE = light rare earth element; MORB = mid-ocean ridge basalts; SDC = Sheeted Dike Complex; UAE = United Arab Emirates; OIB = ocean island basalts; GLOSS = global subducting sediment.

heavy REEs, resulting in a decrease in Dy/Yb with increasing amphibole fractionation (Davidson et al., 2007; Macpherson et al., 2006). Phase 2 intrusions record a negative correlation between Dy/Yb and SiO<sub>2</sub>, defining an amphibole dominated fractionation trend similar to that of the Lesser Antilles (Davidson et al., 2007; Figure 11a). Accessory phases such as apatite and zircon may also affect REE patterns, however, these phases typically crystallize only from more evolved magmas (Davidson et al., 2007). Moreover, Y, which is largely incompatible in typical anhydrous assemblages, but compatible in amphibole (Davidson et al., 2007), records a distinct relative depletion in the Phase 2 sample series (Figure 7). On a plot of Y versus SiO<sub>2</sub> (Figure 11b) Phase 1 samples follow more anhydrous fractionation trends extending to higher Y values with increasing differentiation. In contrast, Phase 2 samples extend to lower Y content with the more evolved GT-tonalites having Y contents as low as <10 ppm at >75 wt% SiO<sub>2</sub>. This strongly suggests the involvement of amphibole during fractionation (Klaver et al., 2018). To further support this the difference between observed and expected values of the MREEs ( $Dy/Dy^* = Dy_n / (La_n^{4/13}/Yb_n^{9/13})$ ) is shown in Figure 11c. This ratio quantifies the extent of MREE depletion (Davidson et al., 2012;

Figure 11c). The trends exhibited by Phase 2 follow amphibole fractionation trends that extend outside the MORB field. This contrasts with Phase 1 and Phase 3 literature data (Godard et al., 2006; Haase et al., 2015). Phase 1 is within the MORB field, whereas Phase 3 shows the influence of sediment material, plotting around GLOSS with a pronounced MREE depletion. The data presented in Figure 11 strongly suggest Phase 2 to be dominated by hydrous, amphibole-bearing fractionation trends commonly exhibited by arc volcanoes (Figure 11; Davidson et al., 2007). Interestingly the Phase 1 samples presented in this study also appear to record an arc-signature, as variation in Dy/Yb and Dy/Dy\* follows the same trend as Phase 2. These samples are also notably enriched in fluid mobile elements, record a slight positive Zr and Hf anomaly (Figure 7) and contain noticeably more iron oxide phases than that documented in the literature (e.g., Lippard et al., 1986). With the recognition that Phase 1 records a subduction signature (e.g., Goodenough et al., 2010, 2014; Ishikawa et al., 2002; Lachize et al., 1996; MacLeod et al., 2013), these specific Phase 1 samples, possibly indicate that Phase 1 can locally exhibit more pronounced arc signatures.

Although the petrography and trace element data indicate amphibole fractionation in Phase 2 magmas, extensive amphibole cumulates are not found in the ophiolite. Arc volcanic suites typically obtain their geochemical amphibole signature through the reaction of melts with earlier-formed cumulate mushes to form amphibole in the lower crust; a process that drives the generation of intermediate and felsic magmas (Davidson et al., 2007, 2012; Klaver et al., 2017, 2018; Smith, 2014). These crystal-poor felsic melts ascend to shallower levels where amphibole might not be stable as phenocryst phase, thus giving rise to the concept of cryptic amphibole fractionation (Davidson et al., 2007). The presence of amphibole has been reported in the Oman-UAE ophiolite (e.g., Goodenough et al., 2010; Haase et al., 2016; Müller et al., 2017), yet surprisingly its influence on the Phase 2 magmatic suite was not previously considered in detail. Amphibole was either concluded to be stable only in evolved Phase 2 rock types (Haase et al., 2016) or the process stabilizing amphibole could not be identified (Müller et al., 2017). The presence of large amounts of amphibole in the gabbroic samples, decreasing Dy/Yb with increased SiO<sub>2</sub> and low Y contents in the tonalites, suggest that amphibole was stabilized early in the differentiation of the Phase 2 magmas; analogous to hydrous arc magmas. A critical aspect is the identical Pb isotope composition of a tonalite and gabbro sample from the same locality (Figure 10): more so than the similarity in Nd and Hf isotope composition (Figure 9), this indicates that the mafic and felsic Phase 2 samples are cogenetic. Generating the tonalites through partial melting of an amphibole-bearing source (slab, sediments, crust) is clearly inconsistent with the isotopic evidence. The presence of subhedral, possible relic, clinopyroxene indicates that amphibole formed in response to a reaction between a hydrous melt and clinopyroxene bearing cumulates (Best, 1975; Coltorti et al., 2004; Debari et al., 1987; Francis, 1976; Klaver et al., 2017; Neal, 1988; Smith, 2014). Moreover, the observed increase in LREE with decreasing MgO indicates fractional crystallization of a mafic magma, producing tonalitic compositions (Figure 8a; Brophy, 2008, 2009; Brophy & Pu, 2012). Concomitantly, we conclude that the GT-compositions are a product of the reaction of an ascending hydrous melt with clinopyroxene/olivine bearing cumulates, the latter likely being the Phase 1 crustal succession. The stabilization of amphibole rapidly increased the SiO<sub>2</sub> content of the derivative melt and gave way to the formation of tonalitic compositions. These tonalites generally form close to the surface, while the microgabbros formed deeper in the ophiolite and likely represent the melt channels that fed Phase 2 magmas to the surface. The GT-gabbros form the hybrid melt compositions between these two rock types as this accounts for the low TiO<sub>2</sub> (Figures 4 and 6), presence of quartz (see petrography) and the observed intermediate composition between the microgabbros and GT-tonalites for all elemental compositions (Figures 4–7).

The processes described here closely resemble the “amphibole sponge” scenario envisaged for arc settings (Davidson et al., 2007; Klaver et al., 2018; Smith, 2014). The crucial difference between arc settings and the Oman-UAE ophiolite is the crustal thickness. Amphibole stability increases with pressure and hence it is generally believed that cumulate-melt reactions to form amphibole are restricted to the lower to middle crust of continental arcs (e.g., Annen et al., 2005; Klaver et al., 2018). Alternatively, high Na<sub>2</sub>O contents can promote amphibole stability and thus allow an amphibole sponge to form at lower pressure in an island arc (Smith, 2014). This clearly contrasts with the thin oceanic crust of the Oman-UAE ophiolite and low Na<sub>2</sub>O contents in the depleted primary magmas. Hence, an important implication of our study is that high H<sub>2</sub>O contents allow amphibole-forming reactions with ultramafic cumulates to occur even at low pressures in oceanic crust.

## 7. Conclusions

The detailed description of later stage intrusions in the northern, central, and southern part of the ophiolite establishes similar field and petrographic relationships and major, trace, and isotopic compositions to Phase 2 intrusions documented in the literature. The abundance of these intrusions in the south conflicts with the assumption that Phase 2 magmatism is less pronounced in that part of the ophiolite (e.g., Goodenough et al., 2014; Nicolle et al., 2016) and argues for a widespread distribution of this type of magmatism.

Phase 2 magmatism varies in composition from primitive microgabbros to more evolved tonalites, while being associated with wehrlite cumulates. This type of magmatism is characterized by amphibole fractionation, low TiO<sub>2</sub> content, LREE depletion, enrichment in 2+ cations Ba and Sr, Th enrichment over Nb, more radiogenic Pb isotope compositions of plagioclase, and similar εHf and εNd compositions when compared to Phase 1. We suggest these geochemical variations were a direct consequence of hydrous partial melting of the depleted mantle source from which Phase 1 originated. The fluid that hydrated the source was likely derived from fluid metasomatism of the mantle wedge and marks the onset of arc-like magmatism across the entire Oman-UAE ophiolite. The widespread nature of Phase 2 magmatism and subduction signature already present in Phase 1 magmatism (MacLeod et al., 2013, and this study) argues that the entire ophiolite formed in a (young) SSZ setting.

## Acknowledgments

We thank Richard Smeets, Bas van der Wagt, and Roel van Elsas for their assistance with sample preparation and analytical procedures. Fruitful discussions were conducted with Edgar Steenstra, Pim Kaskes, and Hidde de Graaff. David Schofield and Mike Styles of the British Geological Survey are thanked for discussions in the field. Michel Grégoire and an anonymous reviewer are thanked for their constructive criticism. K.G. publishes with the permission of the Executive Director of the British Geological Survey. All data used are listed in the references and supplements.

## References

- Abily, B., & Ceuleneer, G. (2013). The dunitic mantle-crust transition zone in the Oman ophiolite: Residue of melt-rock interaction, cumulates from high-MgO melts, or both? *Geology*, *41*(1), 67–70. <https://doi.org/10.1130/G33351.1>
- Abily, B., Ceuleneer, G., & Launeau, P. (2011). Synmagmatic normal faulting in the lower oceanic crust: Evidence from the Oman ophiolite. *Geology*, *39*(4), 391–394. <https://doi.org/10.1130/G31652.1>
- Adachi, Y., & Miyashita, S. (2003). Geology and petrology of the plutonic complexes in the Wadi Fizh area: Multiple magmatic events and segment structure in the northern Oman ophiolite. *Geochemistry, Geophysics, Geosystems*, *4*(9), 8619. <https://doi.org/10.1029/2001GC000272>
- Alabaster, T., Pearce, J. A., & Malpas, J. (1982). The volcanic stratigraphy and petrogenesis of the Oman ophiolite complex. *Contributions to Mineralogy and Petrology*, *81*(3), 168–183. <https://doi.org/10.1007/BF00371294>
- Alonso-Perez, R., Müntener, O., & Ulmer, P. (2009). Igneous garnet and amphibole fractionation in the roots of island arcs: Experimental constraints on andesitic liquids. *Contributions to Mineralogy and Petrology*, *157*(4), 541–558. <https://doi.org/10.1007/s00410-008-0351-8>
- Annen, C., Blundy, J. D., & Sparks, R. S. J. (2005). The genesis of intermediate and silicic magmas in deep crustal hot zones. *Journal of Petrology*, *47*(3), 505–539.
- Anonymous (1972). Penrose field conference on ophiolites. *Geotimes*, *17*, 24–25.
- Arculus, R. J. (2003). Use and abuse of the terms calcalkaline and calcalkalic. *Journal of Petrology*, *44*(5), 929–935. <https://doi.org/10.1093/petrology/44.5.929>
- Bédard, J. H. (2006). Trace element partitioning in plagioclase feldspar. *Geochimica et Cosmochimica Acta*, *70*, 3717–3742. <https://doi.org/10.1016/j.gca.2006.05.003>
- Benoit, M., Ceuleneer, G., & Polvé, M. (1999). The remelting of hydrothermally altered peridotite at mid-ocean ridges by intruding mantle diapirs. *Nature*, *402*(6761), 514–518. <https://doi.org/10.1038/990073>
- Benoit, M., Polvé, M., & Ceuleneer, G. (1996). Trace element and isotopic characterization of mafic cumulates in a fossil mantle diapir (Oman ophiolite). *Chemical Geology*, *134*(1–3), 199–214. [https://doi.org/10.1016/S0009-2541\(96\)00087-3](https://doi.org/10.1016/S0009-2541(96)00087-3)
- Best, M. G. (1975). Amphibole-bearing cumulate inclusions, Grand Canyon, Arizona and their bearing on silica-undersaturated hydrous magmas in the upper mantle. *Journal of Petrology*, *16*(1), 212–236. <https://doi.org/10.1093/petrology/16.1.212>
- Borisova, A. Y., Ceuleneer, G., Kamenetsky, V. S., Arai, S., Bějina, F., Abily, B., et al. (2012). A new view on the petrogenesis of the Oman ophiolite chromitites from microanalyses of chromite-hosted inclusions. *Journal of Petrology*, *53*(12), 2411–2440. <https://doi.org/10.1093/petrology/egs054>
- Bosch, D., Jamais, M., Boudier, F., Nicolas, A., Dautria, J. M., & Agrinier, P. (2004). Deep and high-temperature hydrothermal circulation in the Oman ophiolite—Petrological and isotopic evidence. *Journal of Petrology*, *45*(6), 1181–1208. <https://doi.org/10.1093/petrology/egh010>
- Boudier, F., Godard, M., & Armbruster, C. (2000). Significance of gabbro occurrence in the crustal section of the Semail ophiolite. *Marine Geophysical Research*, *21*(3/4), 307–326. <https://doi.org/10.1023/A:1026726232402>
- Boudier, F., & Juteau, T. (2000). The ophiolite of Oman and United Arab Emirates. *Marine Geophysical Research*, *21*(3/4), 145–146. <https://doi.org/10.1023/A:1026754209262>
- Boudier, F., & Nicolas, A. (1995). Nature of the Moho transition zone in the Oman ophiolite. *Journal of Petrology*, *36*(3), 777–796. <https://doi.org/10.1093/petrology/36.3.777>
- Bralower, T. J., Fullagar, P. D., Paull, C. K., Dwyer, G. S., & Leckie, R. M. (1997). Mid-Cretaceous strontium-isotope stratigraphy of deep-sea sections. *Geological Society of America Bulletin*, *109*(11), 1421–1442. [https://doi.org/10.1130/0016-7606\(1997\)109<1421:MCSISO>2.3.CO;2](https://doi.org/10.1130/0016-7606(1997)109<1421:MCSISO>2.3.CO;2)
- Brophy, J. G. (2008). A study of rare earth element (REE)–SiO<sub>2</sub> variations in felsic liquids generated by basalt fractionation and amphibolite melting: A potential test for discriminating between the two different processes. *Contributions to Mineralogy and Petrology*, *156*(3), 337–357. <https://doi.org/10.1007/s00410-008-0289-x>
- Brophy, J. G. (2009). La–SiO<sub>2</sub> and Yb–SiO<sub>2</sub> systematics in mid-ocean ridge magmas: Implications for the origin of oceanic plagiogranite. *Contributions to Mineralogy and Petrology*, *158*(1), 99–111. <https://doi.org/10.1007/s00410-008-0372-3>
- Brophy, J. G., & Pu, X. (2012). Rare earth element–SiO<sub>2</sub> systematics of mid-ocean ridge plagiogranites and host gabbros from the Fournier oceanic fragment, New Brunswick, Canada: A field evaluation of some model predictions. *Contributions to Mineralogy and Petrology*, *164*(2), 191–204. <https://doi.org/10.1007/s00410-012-0732-x>

- Cawthorn, R. G., & O'hara, M. J. (1976). Amphibole fractionation in calc-alkaline magma genesis. *American Journal of Science*, 276(3), 309–329. <https://doi.org/10.2475/ajs.276.3.309>
- Coleman, R. G. (1981). Tectonic setting for ophiolite obduction in Oman. *Journal of Geophysical Research*, 86(B4), 2497–2508. <https://doi.org/10.1029/JB086iB04p02497>
- Coltorti, M., Beccaluva, L., Bonadiman, C., Faccini, B., Ntaflos, T., & Siena, F. (2004). Amphibole genesis via metasomatic reaction with clinopyroxene in mantle xenoliths from Victoria Land, Antarctica. *Lithos*, 75(1–2), 115–139. <https://doi.org/10.1016/j.lithos.2003.12.021>
- Davidson, J., Turner, S., Handley, H., Macpherson, C., & Dosseto, A. (2007). Amphibole “sponge” in arc crust? *Geology*, 35(9), 787–790. <https://doi.org/10.1130/G23637A.1>
- Davidson, J., Turner, S., & Plank, T. (2012). Dy/Dy\*: Variations arising from mantle sources and petrogenetic processes. *Journal of Petrology*, 54(3), 525–537.
- Debari, S., Kay, S. M., & Kay, R. W. (1987). Ultramafic xenoliths from Adagdak volcano, Adak, Aleutian Islands, Alaska: Deformed igneous cumulates from the Moho of an island arc. *The Journal of Geology*, 95(3), 329–341. <https://doi.org/10.1086/629133>
- Dilek, Y., & Flower, M. F. (2003). Arc-trench rollback and forearc accretion: 2. A model template for ophiolites in Albania, Cyprus, and Oman. *Geological Society, London, Special Publications*, 218(1), 43–68. <https://doi.org/10.1144/GSL.SP.2003.218.01.04>
- Eggins, S. M., Woodhead, J. D., Kinsley, L. P. J., Mortimer, G. E., Sylvester, P., McCulloch, M. T., et al. (1997). A simple method for the precise determination of  $\geq 40$  trace elements in geological samples by ICPMS using enriched isotope internal standardisation. *Chemical Geology*, 134(4), 311–326. [https://doi.org/10.1016/S0009-2541\(96\)00100-3](https://doi.org/10.1016/S0009-2541(96)00100-3)
- Einaudi, F., Pezard, P. A., Cochemé, J. J., Coulon, C., Laverne, C., & Godard, M. (2000). Petrography, geochemistry and physical properties of a continuous extrusive section from the Sarami Massif, Semail ophiolite. *Marine Geophysical Researches*, 21(3/4), 387–408. <https://doi.org/10.1023/A:1026752415989>
- Elliott, T. (2003). Tracers of the slab. In J. Eiler (Ed.), *Geophysical monograph* (Vol. 138, pp. 23–46). Washington, DC: American Geophysical Union.
- Ernewein, M., Pflumio, C., & Whitechurch, H. (1988). The death of an accretion zone as evidenced by the magmatic history of the Sumail ophiolite (Oman). *Tectonophysics*, 151(1–4), 247–274. [https://doi.org/10.1016/0040-1951\(88\)90248-X](https://doi.org/10.1016/0040-1951(88)90248-X)
- Francis, D. M. (1976). Amphibole pyroxenite xenoliths: Cumulate or replacement phenomena from the upper mantle, Nunivak Island, Alaska. *Contributions to Mineralogy and Petrology*, 58(1), 51–61. <https://doi.org/10.1007/BF00384744>
- Garrido, C. J., Kelemen, P. B., & Hirth, G. (2001). Variation of cooling rate with depth in lower crust formed at an oceanic spreading ridge: Plagioclase crystal size distributions in gabbros from the Oman ophiolite. *Geochemistry, Geophysics, Geosystems*, 2(10). <https://doi.org/10.1029/2000GC000136>
- Ghiorso, M. S., & Gualda, G. A. (2015). An H<sub>2</sub>O–CO<sub>2</sub> mixed fluid saturation model compatible with rhyolite–MELTS. *Contributions to Mineralogy and Petrology*, 169(6), 53. <https://doi.org/10.1007/s00410-015-1141-8>
- Godard, M., Bosch, D., & Einaudi, F. (2006). A MORB source for low-Ti magmatism in the Semail ophiolite. *Chemical Geology*, 234(1–2), 58–78. <https://doi.org/10.1016/j.chemgeo.2006.04.005>
- Godard, M., Dautria, J. M., & Perrin, M. (2003). Geochemical variability of the Oman ophiolite lavas: Relationship with spatial distribution and paleomagnetic directions. *Geochemistry, Geophysics, Geosystems*, 4(6), 8609. <https://doi.org/10.1029/2002GC000452>
- Goodenough, K. M., Styles, M. T., Schofield, D., Thomas, R. J., Crowley, Q. C., Lilly, R. M., et al. (2010). Architecture of the Oman–UAE ophiolite: Evidence for a multi-phase magmatic history. *Arabian Journal of Geosciences*, 3(4), 439–458. <https://doi.org/10.1007/s12517-010-0177-3>
- Goodenough, K. M., Thomas, R. J., Styles, M. T., Schofield, D. I., & MacLeod, C. J. (2014). Records of ocean growth and destruction in the Oman–UAE ophiolite. *Elements*, 10(2), 109–114. <https://doi.org/10.2113/gselements.10.2.109>
- Griselin, M., Van Belle, J. C., Pomies, C., Vroon, P. Z., Van Soest, M. C., & Davies, G. R. (2001). An improved chromatographic separation technique of Nd with application to NdO<sup>+</sup> isotope analysis. *Chemical Geology*, 172(3–4), 347–359. [https://doi.org/10.1016/S0009-2541\(00\)00256-4](https://doi.org/10.1016/S0009-2541(00)00256-4)
- Haase, K. M., Freund, S., Beier, C., Koepke, J., Erdmann, M., & Hauff, F. (2016). Constraints on the magmatic evolution of the oceanic crust from plagiogranite intrusions in the Oman ophiolite. *Contributions to Mineralogy and Petrology*, 171(5), 1–16.
- Haase, K. M., Freund, S., Koepke, J., Hauff, F., & Erdmann, M. (2015). Melts of sediments in the mantle wedge of the Oman ophiolite. *Geology*, 43(4), 275–278. <https://doi.org/10.1130/G36451.1>
- Hacker, B. R., Mosenfelder, J. L., & Gnos, E. (1996). Rapid emplacement of the Oman ophiolite: Thermal and geochronologic constraints. *Tectonics*, 15(6), 1230–1247. <https://doi.org/10.1029/96TC01973>
- Hastie, A. R., Kerr, A. C., Pearce, J. A., & Mitchell, S. F. (2007). Classification of altered volcanic island arc rocks using immobile trace elements: Development of the Th–Co discrimination diagram. *Journal of Petrology*, 48(12), 2341–2357. <https://doi.org/10.1093/petrology/egm062>
- Irvine, T. N. J., & Baragar, W. R. A. F. (1971). A guide to the chemical classification of the common volcanic rocks. *Canadian Journal of Earth Sciences*, 8(5), 523–548. <https://doi.org/10.1139/e71-055>
- Ishikawa, T., Nagaishi, K., & Umino, S. (2002). Boninitic volcanism in the Oman ophiolite: Implications for thermal condition during transition from spreading ridge to arc. *Geology*, 30(10), 899–902. [https://doi.org/10.1130/0091-7613\(2002\)030<0899:BVITOO>2.0.CO;2](https://doi.org/10.1130/0091-7613(2002)030<0899:BVITOO>2.0.CO;2)
- Jansen, M. N., Lissenberg, C. J., Klaver, M., de Graaff, S. J., Koornneef, J. M., Smeets, R. J., et al. (2018). Isotopic variation in Semail ophiolite lower crust reveals crustal-level melt aggregation. *Geochemical Perspectives Letters*, 8, 37–42.
- Juteau, T., Ernewein, M., Reuber, I., Whitechurch, H., & Dahl, R. (1988). Duality of magmatism in the plutonic sequence of the Sumail Nappe, Oman. *Tectonophysics*, 151(1–4), 107–135. [https://doi.org/10.1016/0040-1951\(88\)90243-0](https://doi.org/10.1016/0040-1951(88)90243-0)
- Kawahata, H., Nohara, M., Ishizuka, H., Hasebe, S., & Chiba, H. (2001). Sr isotope geochemistry and hydrothermal alteration of the Oman ophiolite. *Journal of Geophysical Research*, 106(B6), 11,083–11,099. <https://doi.org/10.1029/2000JB900456>
- Kinzler, R. J., & Grove, T. L. (1993). Corrections and further discussion of the primary magmas of mid-ocean ridge basalts, 1 and 2. *Journal of Geophysical Research*, 98(B12), 22,339–22,347. <https://doi.org/10.1029/93JB02164>
- Klaver, M., Blundy, J. D., & Vroon, P. Z. (2018). Generation of arc rhyodacites through cumulate–melt reactions in a deep crustal hot zone: Evidence from Nisyros volcano. *Earth and Planetary Science Letters*, 497, 169–180. <https://doi.org/10.1016/j.epsl.2018.06.019>
- Klaver, M., Carey, S., Nomikou, P., Smet, I., Godelitsas, A., & Vroon, P. (2016). A distinct source and differentiation history for Kolumbo submarine volcano, Santorini volcanic field, Aegean arc. *Geochemistry, Geophysics, Geosystems*, 17, 3254–3273. <https://doi.org/10.1002/2016GC006398>
- Klaver, M., Davies, G. R., & Vroon, P. Z. (2016). Subslab mantle of African provenance infiltrating the Aegean mantle wedge. *Geology*, 44(5), 367–370. <https://doi.org/10.1130/G37627.1>

- Klaver, M., Matveev, S., Berndt, J., Lissenberg, C. J., & Vroon, P. Z. (2017). A mineral and cumulate perspective to magma differentiation at Nisyros volcano, Aegean arc. *Contributions to Mineralogy and Petrology*, *172*(11–12), 95. <https://doi.org/10.1007/s00410-017-1414-5>
- Klaver, M., Smeets, R. J., Koornneef, J. M., Davies, G. R., & Vroon, P. Z. (2016). Pb isotope analysis of ng size samples by TIMS equipped with a  $10^{13}$   $\Omega$  resistor using a  $^{207}\text{Pb}$ - $^{204}\text{Pb}$  double spike. *Journal of Analytical Atomic Spectrometry*, *31*, 171–178. <https://doi.org/10.1039/C5JA00130G>
- Koepke, J., Schoenborn, S., Oelze, M., Wittmann, H., Feig, S. T., Hellebrand, E., et al. (2009). Petrogenesis of crustal wehrlites in the Oman ophiolite: Experiments and natural rocks. *Geochemistry, Geophysics, Geosystems*, *10*, Q10002. <https://doi.org/10.1029/2009GC002488>
- Koga, K. T., Kelemen, P. B., & Shimizu, N. (2001). Petrogenesis of the crust-mantle transition zone and the origin of lower crustal wehrlite in the Oman ophiolite. *Geochemistry, Geophysics, Geosystems*, *2*(9). <https://doi.org/10.1029/2000GC000132>
- Lachize, M., Lorand, J. P., & Juteau, T. (1996). Calc-alkaline differentiation trend in the plutonic sequence of the Wadi Haymiliyah section, Haylayn massif, Semail ophiolite, Oman. *Lithos*, *38*(3–4), 207–232. [https://doi.org/10.1016/0024-4937\(96\)00009-6](https://doi.org/10.1016/0024-4937(96)00009-6)
- Langmuir, C. H., Klein, E. M., & Plank, T. (1992). Petrological systematics of mid-ocean ridge basalts: Constraints on melt generation beneath ocean ridges. In J. P. Morgan, D. K. Blackman, & J. M. Sinton (Eds.), *Mantle flow and melt generation at mid-ocean ridges* (Vol. 71, pp. 183–280). Washington, D. C: American Geophysical Union.
- Le Maitre, R. W., Streckeisen, A., Zanettin, B., Le Bas, M. J., Bonin, B., & Bateman, P. (Eds.). (2005). *Igneous rocks: A classification and glossary of terms: Recommendations of the International Union of Geological Sciences Subcommittee on the Systematics of Igneous Rocks*. Cambridge: Cambridge University Press.
- Lehnert, K., Su, Y., Langmuir, C. H., Sarbas, B., & Nohl, U. (2000). A global geochemical database structure for rocks. *Geochemistry, Geophysics, Geosystems*, *1*(5). <https://doi.org/10.1029/1999GC000026>
- Lippard, S. J., Shelton, A. W., & Gass, I. G. (1986). *The ophiolite of northern Oman, Memoir* (Vol. 11). London: Geological Society.
- MacLeod, C. J., Lissenberg, C. J., & Bibby, L. E. (2013). “Moist MORB” axial magmatism in the Oman ophiolite: The evidence against a mid-ocean ridge origin. *Geology*, *41*, 459–462. <https://doi.org/10.1130/G33904.1>
- MacLeod, C. J., & Yaouancq, G. (2000). A fossil melt lens in the Oman ophiolite: Implications for magma chamber processes at fast spreading ridges. *Earth and Planetary Science Letters*, *176*(3–4), 357–373. [https://doi.org/10.1016/S0012-821X\(00\)00200-0](https://doi.org/10.1016/S0012-821X(00)00200-0)
- Macpherson, C. G., Dreher, S. T., & Thirlwall, M. F. (2006). Adakites without slab melting: High pressure differentiation of island arc magma, Mindanao, the Philippines. *Earth and Planetary Science Letters*, *243*(3–4), 581–593. <https://doi.org/10.1016/j.epsl.2005.12.034>
- Mahoney, J. J., Frei, R., Tejada, M. L. G., Mo, X. X., Leat, P. T., & Nägler, T. F. (1998). Tracing the Indian Ocean mantle domain through time: Isotopic results from old west Indian, east Tethyan, and South Pacific seafloor. *Journal of Petrology*, *39*(7), 1285–1306. <https://doi.org/10.1093/ptro/39.7.1285>
- McArthur, J. M., Howarth, R. J., & Shields, G. A. (2012). Strontium isotope stratigraphy. In F. M. Gredstein, J. G. Ogg, M. D. Schmotz, & G. M. Ogg (Eds.), *The geologic time scale* (pp. 127–144). Amsterdam, Netherlands: Elsevier. <https://doi.org/10.1016/B978-0-444-59425-9.00007-X>
- Melekhova, E., Blundy, J., Robertson, R., & Humphreys, M. C. (2015). Experimental evidence for polybaric differentiation of primitive arc basalt beneath St. Vincent, Lesser Antilles. *Journal of Petrology*, *56*(1), 161–192. <https://doi.org/10.1093/ptro/egu074>
- Miyashiro, A. (1974). Volcanic rock series in island arcs and active continental margins. *American Journal of Science*, *274*, 321–355. <https://doi.org/10.2475/ajs.274.4.321>
- Morris, A., Meyer, M., Anderson, M. W., & MacLeod, C. J. (2016). Clockwise rotation of the entire Oman ophiolite occurred in a supra-subduction zone setting. *Geology*, *44*(12), 1055–1058. <https://doi.org/10.1130/G38380.1>
- Müller, T., Koepke, J., Garbe-Schönberg, C. D., Dietrich, M., Bauer, U., & Wolff, P. E. (2017). Anatomy of a frozen axial melt lens from a fast-spreading paleo-ridge (Wadi Gideah, Oman ophiolite). *Lithos*, *272*, 31–45.
- Münker, C., Weyer, S., Scherer, E., & Mezger, K. (2001). Separation of high field strength elements (Nb, Ta, Zr, Hf) and Lu from rock samples for MC-ICPMS measurements. *Geochemistry, Geophysics, Geosystems*, *2*(12). <https://doi.org/10.1029/2001GC000183>
- Nandedkar, R. H., Ulmer, P., & Müntener, O. (2014). Fractional crystallization of primitive, hydrous arc magmas: An experimental study at 0.7 GPa. *Contributions to Mineralogy and Petrology*, *167*(6), 1015. <https://doi.org/10.1007/s00410-014-1015-5>
- Neal, C. R. (1988). The origin and composition of metasomatic fluids and amphiboles beneath Malaita, Solomon Islands. *Journal of Petrology*, *29*(1), 149–179. <https://doi.org/10.1093/ptro/29.1.149>
- Nicolas, A. (1989). *Structures of ophiolites and dynamics of oceanic lithosphere* (367 pp.). Dordrecht, Netherlands: Kluwer Academic Publishers. <https://doi.org/10.1007/978-94-009-2374-4>
- Nebel, O., Vroon, P. Z., van Westrenen, W., Iizuka, T., & Davies, G. R. (2011). The effect of sediment recycling in subduction zones on the Hf isotope character of new arc crust, Banda arc, Indonesia. *Earth and Planetary Science Letters*, *303*(3), 240–250.
- Nicolas, A., & Boudier, F. (2011). Structure and dynamics of ridge axial melt lenses in the Oman ophiolite. *Journal of Geophysical Research*, *116*, B03103. <https://doi.org/10.1029/2010JB007934>
- Nicolas, A., & Boudier, F. (2015). Inside the magma chamber of a dying ridge segment in the Oman ophiolite. *Terra Nova*, *27*(1), 69–76. <https://doi.org/10.1111/ter.12130>
- Nicolas, A., Boudier, F., & Ildefonse, B. (1996). Variable crustal thickness in the Oman ophiolite: Implication for oceanic crust. *Journal of Geophysical Research*, *101*(B8), 17,941–17,950. <https://doi.org/10.1029/96JB00195>
- Nicolas, A., Mainprice, D., & Boudier, F. (2003). High-temperature seawater circulation throughout crust of oceanic ridges: A model derived from the Oman ophiolites. *Journal of Geophysical Research*, *108*(B8), 2371. <https://doi.org/10.1029/2002JB002094>
- Nicolle, M., Jousset, D., Reisberg, L., Bosch, D., & Stephant, A. (2016). Major and trace element and Sr and Nd isotopic results from mantle diapirs in the Oman ophiolite: Implications for off-axis magmatic processes. *Earth and Planetary Science Letters*, *437*, 138–149. <https://doi.org/10.1016/j.epsl.2015.12.005>
- Nobre Silva, I. G., Weis, D., & Scoates, J. S. (2010). Effects of acid leaching on the Sr-Nd-Hf isotopic compositions of ocean island basalts. *Geochemistry, Geophysics, Geosystems*, *11*, Q09011. <https://doi.org/10.1029/2010GC003176>
- Nowell, G., & Parrish, R. R. (2001). Simultaneous acquisition of isotope compositions and parent/daughter ratios by non-isotope dilution-mode Plasma Ionisation Multi-collector Mass Spectrometry (PIMMS). *Special Publication-Royal Society Of Chemistry*, *267*(1), 298–310.
- Othman, D. B., White, W. M., & Patchett, J. (1989). The geochemistry of marine sediments, island arc magma genesis, and crust-mantle recycling. *Earth and Planetary Science Letters*, *94*(1–2), 1–21. [https://doi.org/10.1016/0012-821X\(89\)90079-4](https://doi.org/10.1016/0012-821X(89)90079-4)
- Pallister, J. S., & Knight, R. J. (1981). Rare-earth element geochemistry of the Samail ophiolite near Ibra, Oman. *Journal of Geophysical Research*, *86*(B4), 2673–2697. <https://doi.org/10.1029/JB086iB04p02673>
- Pearce, J. A. (2008). Geochemical fingerprinting of oceanic basalts with applications to ophiolite classification and the search for Archean oceanic crust. *Lithos*, *100*(1–4), 14–48. <https://doi.org/10.1016/j.lithos.2007.06.016>

- Pearce, J. A. (2014). Immobile element fingerprinting of ophiolites. *Elements*, *10*(2), 101–108. <https://doi.org/10.2113/gselements.10.2.101>
- Pearce, J. A., Alabaster, T., Shelton, A. W., & Searle, M. P. (1981). The Oman ophiolite as a Cretaceous arc-basin complex: Evidence and implications. *Philosophical Transactions of the Royal Society of London A: Mathematical, Physical and Engineering Sciences*, *300*(1454), 299–317. <https://doi.org/10.1098/rsta.1981.0066>
- Plank, T., & Langmuir, C. H. (1998). The chemical composition of subducting sediment and its consequences for the crust and mantle. *Chemical Geology*, *145*(3-4), 325–394. [https://doi.org/10.1016/S0009-2541\(97\)00150-2](https://doi.org/10.1016/S0009-2541(97)00150-2)
- Python, M., & Ceuleneer, G. (2003). Nature and distribution of dykes and related melt migration structures in the mantle section of the Oman ophiolite. *Geochemistry, Geophysics, Geosystems*, *4*(7), 8612. <https://doi.org/10.1029/2002GC000354>
- Python, M., Ceuleneer, G., & Arai, S. (2008). Chromian spinels in mafic-ultramafic mantle dikes: Evidence for a two-stage melt production during the evolution of the Oman ophiolite. *Lithos*, *106*(1-2), 137–154. <https://doi.org/10.1016/j.lithos.2008.07.001>
- Rioux, M., Bowring, S., Kelemen, P., Gordon, S., Dudás, F., & Miller, R. (2012). Rapid crustal accretion and magma assimilation in the Oman-UAE ophiolite: High precision U-Pb zircon geochronology of the gabbroic crust. *Journal of Geophysical Research*, *117*, B07201. <https://doi.org/10.1029/2012JB009273>
- Rioux, M., Bowring, S., Kelemen, P., Gordon, S., Miller, R., & Dudás, F. (2013). Tectonic development of the Samail ophiolite: High-precision U-Pb zircon geochronology and Sm-Nd isotopic constraints on crustal growth and emplacement. *Journal of Geophysical Research: Solid Earth*, *118*, 2085–2101. <https://doi.org/10.1002/jgrb.50139>
- Rollinson, H. (2005). Chromite in the mantle section of the Oman ophiolite: A new genetic model. *Island Arc*, *14*(4), 542–550. <https://doi.org/10.1111/j.1440-1738.2005.00482.x>
- Rollinson, H. (2009). New models for the genesis of plagiogranites in the Oman ophiolite. *Lithos*, *112*(3-4), 603–614. <https://doi.org/10.1016/j.lithos.2009.06.006>
- Rollinson, H. (2015). Slab and sediment melting during subduction initiation: Granitoid dikes from the mantle section of the Oman ophiolite. *Contributions to Mineralogy and Petrology*, *170*(3), 32. <https://doi.org/10.1007/s00410-015-1177-9>
- Rollinson, H., & Adetunji, J. (2013). Mantle podiform chromitites do not form beneath mid-ocean ridges: A case study from the Moho transition zone of the Oman ophiolite. *Lithos*, *177*, 314–327. <https://doi.org/10.1016/j.lithos.2013.07.004>
- Rospabé, M., Ceuleneer, G., Benoit, M., Abily, B., & Pinet, P. (2017). Origin of the dunitic mantle-crust transition zone in the Oman ophiolite: The interplay between percolating magmas and high-temperature hydrous fluids. *Geology*, *45*(5), 471–474. <https://doi.org/10.1130/G38778.1>
- Shervais, J. W. (2001). Birth, death, and resurrection: The life cycle of suprasubduction zone ophiolites. *Geochemistry, Geophysics, Geosystems*, *2*(1). <https://doi.org/10.1029/2000GC000080>
- Sisson, T. W., & Grove, T. L. (1993). Experimental investigations of the role of H<sub>2</sub>O in calc-alkaline differentiation and subduction zone magmatism. *Contributions to Mineralogy and Petrology*, *113*(2), 143–166. <https://doi.org/10.1007/BF00283225>
- Smith, D. J. (2014). Clinopyroxene precursors to amphibole sponge in arc crust. *Nature Communications*, *5*, 4329. <https://doi.org/10.1038/ncomms5329>
- Staudigel, H., Plank, T., White, B., & Schmincke, H. U. (1996). Geochemical fluxes during seafloor alteration of the basaltic upper oceanic crust: DSDP Sites 417 and 418. In G. E. Bebout, D. W. Scholl, S. H. Kirby, & J. P. Platt (Eds.), *Subduction top to bottom* (pp. 19–38). Washington, D.C: American Geophysical Union.
- Stille, P., Steinmann, M., & Riggs, S. R. (1996). Nd isotope evidence for the evolution of the paleocurrents in the Atlantic and Tethys Oceans during the past 180 Ma. *Earth and Planetary Science Letters*, *144*(1–2), 9–19. [https://doi.org/10.1016/0012-821X\(96\)00157-4](https://doi.org/10.1016/0012-821X(96)00157-4)
- Styles, M., Ellison, R., Arkley, S., Crowley, Q. G., Farrant, A., Goodenough, K. M., et al. (2006). *The geology and geophysics of the United Arab Emirates: Volume 2, geology*, (p. 351). Abu Dhabi, United Arab Emirates, United Arab Emirates: Ministry of Energy, Petroleum and Minerals Sector, Minerals Department.
- Sun, S. S., & McDonough, W. S. (1989). Chemical and isotopic systematics of oceanic basalts: Implications for mantle composition and processes. *Geological Society, London, Special Publications*, *42*(1), 313–345. <https://doi.org/10.1144/GSL.SP.1989.042.01.19>
- Warren, C. J., Parrish, R. R., Waters, D. J., & Searle, M. P. (2005). Dating the geologic history of Oman's Semail ophiolite: Insights from U-Pb geochronology. *Contributions to Mineralogy and Petrology*, *150*(4), 403–422. <https://doi.org/10.1007/s00410-005-0028-5>
- White, W. M., Patchett, J., & Ben Othman, D. (1986). Hf isotope ratios of marine sediments and Mn nodules: Evidence for a mantle source of Hf in seawater. *Earth and Planetary Science Letters*, *79*(1–2), 46–54. [https://doi.org/10.1016/0012-821X\(86\)90039-7](https://doi.org/10.1016/0012-821X(86)90039-7)
- Whitney, D. L., & Evans, B. W. (2010). Abbreviations for names of rock-forming minerals. *American Mineralogist*, *95*(1), 185–187. <https://doi.org/10.2138/am.2010.3371>
- Workman, R. K., & Hart, S. R. (2005). Major and trace element composition of the depleted MORB mantle (DMM). *Earth and Planetary Science Letters*, *231*(1-2), 53–72. <https://doi.org/10.1016/j.epsl.2004.12.005>
- Yamasaki, T., Maeda, J., & Mizuta, T. (2006). Geochemical evidence in clinopyroxenes from gabbroic sequence for two distinct magmatism in the Oman ophiolite. *Earth and Planetary Science Letters*, *251*(1-2), 52–65. <https://doi.org/10.1016/j.epsl.2006.08.027>